7-Dehydrocholesterol-derived oxysterols cause neurogenic defects in Smith-Lemli-Opitz syndrome

Hideaki Tomita [a], Kelly M. Hines [a,b], Josi M. Herron [a], Amy Li [a], David W. Baggett [a,c], Libin Xu [a,*]

[a] Department of Medicinal Chemistry, University of Washington, Seattle, WA, 98115, USA

[b] Current address: Department of Chemistry, University of Georgia, Athens, GA, 30602, USA

[c] Current address: Department of Structural Biology, St. Jude Children's Research Hospital, Memphis, TN, 38105, USA

*, Correspondence: libinxu@uw.edu

Abstract

Defective 3β-hydroxysterol-Δ^7-reductase (DHCR7) in the developmental disorder, Smith-Lemli-Opitz syndrome (SLOS), results in deficiency in cholesterol and accumulation of its precursor, 7-dehydrocholesterol (7-DHC). Here, we show that loss of *DHCR7* causes accumulation of 7-DHC-derived oxysterol metabolites, premature neurogenesis, and perturbation of neuronal localization in developing murine or human cortical neural precursors, both *in vitro* and *in vivo*. We found that a major oxysterol, 3β,5α-dihydroxycholest-7-en-6-one (DHCEO), mediates these effects by initiating crosstalk between glucocorticoid receptor (GR) and neurotrophin receptor kinase TrkB. Either loss of *DHCR7* or direct exposure to DHCEO causes hyperactivation of GR and TrkB and their downstream MEK-ERK-C/EBP signaling pathway in cortical neural precursors. Moreover, direct inhibition of GR activation with an antagonist or inhibition of DHCEO accumulation with antioxidants rescues the premature neurogenesis phenotype caused by the loss of *DHCR7*. These results suggest that GR could be a new therapeutic target against the neurological defects observed in SLOS.

Keywords: Smith-Lemli-Opitz syndrome, cholesterol, 7-dehydrocholesterol, oxysterol, neurogenesis, neural progenitor, glucocorticoid receptor, TrkB, cortical development

47 **Introduction**

48 Brain is rich in cholesterol, contributing to 25% of total cholesterol in human body, and
49 nearly all cholesterol in the brain is synthesized locally (Dietschy and Turley, 2004). Therefore,
50 dysregulation of cholesterol metabolism in CNS can potentially cause significant defects in CNS
51 development and functions. Indeed, enzymatic deficiencies in cholesterol biosynthesis cause a
52 number of inherited diseases with severe neurodevelopmental phenotypes (Porter and Herman,
53 2011).

54 Smith-Lemli Opitz syndrome (SLOS) is an autosomal recessive, neurological and
55 developmental disorder characterized by multiple developmental defects, such as distinctive
56 facial features, cleft palate, microcephaly and holoprosencephaly, as well as severe intellectual
57 impairment and behavioral problems (Porter and Herman, 2011; Thurm et al., 2016). Notably,
58 SLOS patients display high incidence (> 50%) of autism spectrum disorders (Bukelis et al.,
59 2007; Sikora et al., 2006; Tierney et al., 2006). SLOS is caused by mutations in the 3β-
60 hydroxysterol-Δ^7 -reductase gene (*DHCR7*), which encodes the enzyme that converts 7-
61 dehydrocholesterol (7-DHC) to cholesterol in the final step of the cholesterol biosynthesis
62 pathway (Fitzky et al., 1998; Tint et al., 1994; Wassif et al., 1998). Defective DHCR7 resulting
63 from the mutations leads to deficiency in cholesterol and accumulation of 7-DHC in tissues and
64 fluids of affected individuals (Tint et al., 1994; Tint et al., 1995). 7-DHC was found to be highly
65 reactive toward free radical oxidation, leading to the formation of its oxidative metabolites, *i.e.*,
66 oxysterols (Xu et al., 2009; Xu et al., 2010; Xu et al., 2013; Xu et al., 2011). 7-DHC-derived
67 oxysterols can exert cytotoxicity in neuronal cells, induce gene expression changes, and increase
68 formation of dendritic arborization from cortical neurons (Korade et al., 2010; Xu et al., 2012).
69 Interestingly, increased dendrite and axon formation has also been observed in neurons isolated

70 from *Dhcr7*-KO mouse brain (Jiang et al., 2010). These studies suggest that 7-DHC-derived
71 oxysterols may be underlying the alterations in neuronal processes in SLOS.
72 Cholesterol, 7-DHC, and oxysterols derived from both have been found to play important
73 roles in modulating signaling pathways in developing tissues and organs, such as Hedgehog (Hh)
74 and Wnt signaling pathways (Byrne et al., 2016; Corcoran and Scott, 2006; Huang et al., 2018;
75 Myers et al., 2017; Porter et al., 1996; Raleigh et al., 2018). Related to SLOS, ring-B oxysterols
76 derived from 7-DHC oxidation inhibit Smo in the Hh pathway (Sever et al., 2016). On the other
77 hand, cholesterol was recently found to selectively activate canonical Wnt signaling over non-
78 canonical Wnt signaling (Sheng et al., 2014). However, in human induced pluripotent stem cells
79 (hiPSCs) derived from SLOS patient fibroblasts, accumulation of 7-DHC was found to inhibit
80 Wnt/β-catenin pathway, which contributes to the precocious neuronal specification in SLOS
81 neural progenitors (Francis et al., 2016). Depending on the position of the oxidation, oxysterols
82 have also been shown to bind and activate other signaling molecules and nuclear receptors,
83 including estrogen receptors, liver X receptors, and glucocorticoid receptor (GR), and thus, play
84 important roles in neurodevelopment and diseases (DuSell et al., 2008; Theofilopoulos et al.,
85 2013; Voisin et al., 2017). However, it is unknown how alteration of sterol composition
86 influences neural stem cell/progenitor behaviors during cortical development, and it remains
87 elusive whether neural defects of SLOS is due to deficiency in cholesterol or accumulation of 7-
88 DHC or its oxysterols.
89 Here we examine the effects of *DHCR7* mutations in developing neural precursors,
90 focusing on the cerebral cortex. We demonstrate that 7-DHC-derived oxysterols start to
91 accumulate at embryonic day 12.5 (E12.5) and continue to increase at E14.5 and E16.5, and that
92 loss of *DHCR7* causes decreased proliferation and self-renewal of mouse cortical neural

93 precursors and aberrant premature neurogenesis in both mouse and human neural progenitor cells
94 (NPCs). We then provide evidence that a 7-DHC-derived oxysterol, 3β,5α-dihydroxycholest-7-
95 en-6-one (DHCEO), activates GR and the downstream receptor tyrosine kinases (RTKs)-
96 mediated neurogenic signaling through TrkB, and in doing so, promotes premature NPC
97 differentiation and perturbs neuronal positioning. Either inhibition of GR activation with an
98 antagonist or inhibition of DHCEO accumulation with antioxidants rescues the premature
99 neurogenesis defect.
100

101 **Results**
102
103 ***Dhcr7 is Expressed in Embryonic Cortical Precursors and Neurons of Developing Murine***
104 ***Cortex***

105 To understand the role of *Dhcr7* in neural development, we studied murine developing
106 cortical precursors during embryonic neurogenesis. We first analyzed the expression of *Dhcr7*
107 mRNA during mouse cortical development. RT-PCR analysis showed expression of *Dhcr7* in
108 embryonic day 11 (E11) through postnatal day 0 (P0) cortex (Figure 1A). Quantitative PCR
109 (qPCR) also suggested the stable expression of *Dhcr7* from E11 to E18 (Figure 1B). Western
110 blot analysis further confirmed the presence of Dhcr7 protein in developing cortex (Figure 1C).
111 Immunostaining showed that Dhcr7 was broadly expressed in the developing cortex and was
112 detectable in precursors in the E12 ventricular and subventricular (VZ/SVZ) zones (Figure 1D).
113 Immunostaining of cortical sections of *Dhcr7*-KO mouse brain at E12 with this particular Dhcr7
114 antibody confirmed the antibody specificity against Dhcr7. To further establish the expression of
115 Dhcr7 in neural lineage cells, we analyzed cortical precursor cultures from E12.5, which consists
116 of proliferating radial glial cells that generate neurons in culture (Figure 1E). In the E12.5
117 cortical precursor cultures, Dhcr7+ cells were co-labeled with the precursor markers, Sox2 and

Pax6. Dhcr7 was also co-labeled with the neuronal marker, βIII-tubulin, and the neural lineage marker, Nestin. The results suggested that Dhcr7 was consistently expressed in neural lineage cells, which is consistent with our *in vivo* analysis.

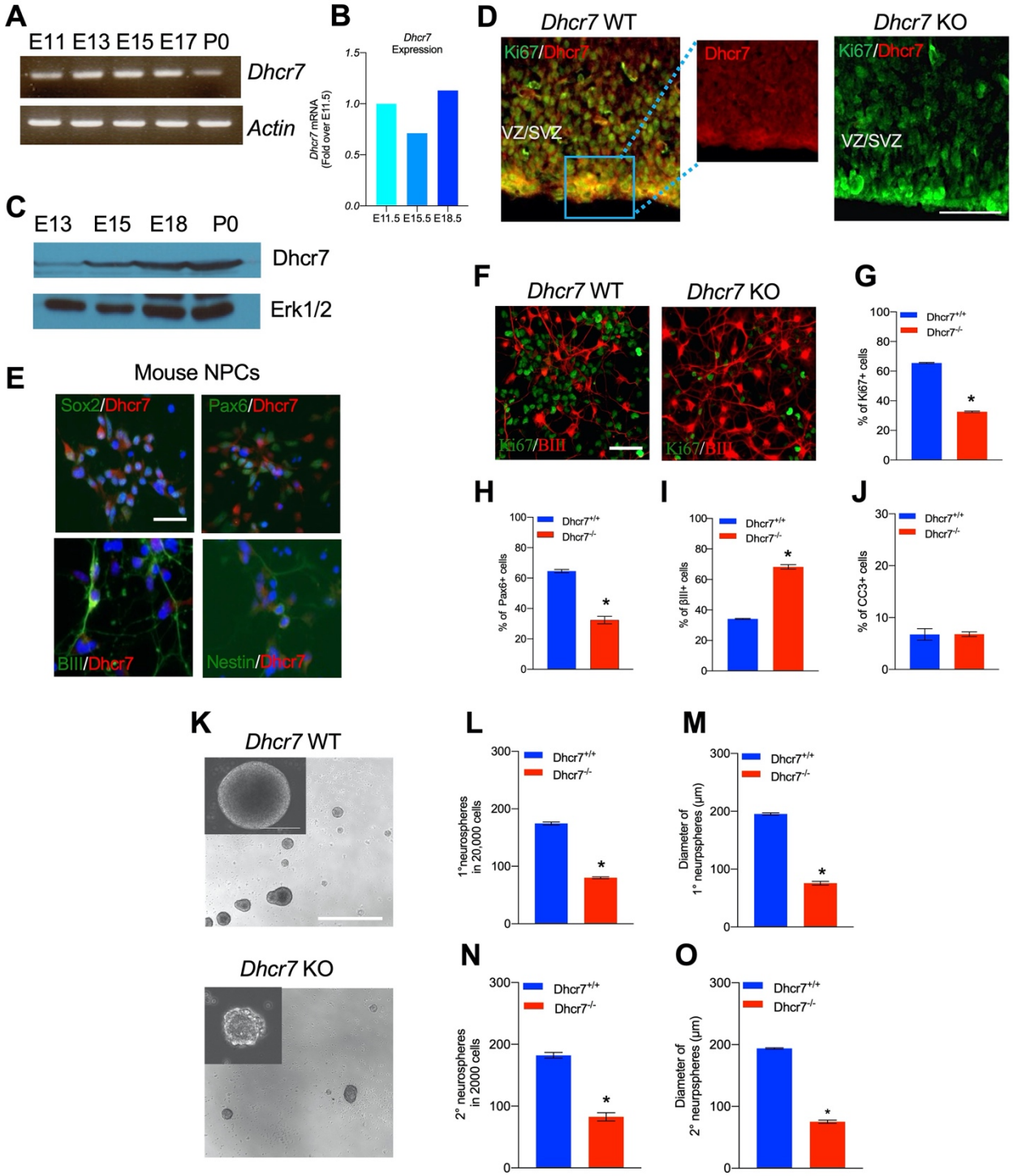

123 **Figure 1. Loss of *Dhcr7* alleles causes decreased proliferation and increased neurogenesis in**
124 **murine cortical precursors.** (A) RT-PCR for *Dhcr7* mRNA in the E11.5 to P0 cortex. *β-actin*
125 mRNA was used as loading control. (B) qRT-PCR for *Dhcr7* mRNA in the E11.5 to E18.5
126 cortex. Data is expressed as fold change over E11.5 cortex. (C) Western blot of Dhcr7 in total
127 cortical lysates from E13.5 to P0. The blot was re-probed for Erk1/2 as a loading control. (D)
128 Images of E13.5 $Dhcr7^{+/+}$ (*Dhcr7*-WT, left panel) and $Dhcr7^{-/-}$ (*Dhcr7*-KO, right panel) cortical
129 sections immunostained for Dhcr7 (red). The subventricular/ventricular zone (SVZ/VZ) is
130 denoted. The right panels show image of boxed area. Scale bar =100 μm. (E) Images of cultured
131 mouse cortical precursors immunostained for Dhcr7 (red) and Sox2, Pax6, βIII-tubulin and
132 Nestin (green) and counterstained with DAPI (blue). Scale bar = 50 μm. (F-J) E12.5 cortical
133 precursors from single $Dhcr^{+/+}$ and $Dhcr7^{-/-}$ embryos were cultured 3 days and analyzed. (F)
134 Cells were immunostained for Ki67 (green) and βIII-tubulin (red) after 3 days and quantified for
135 the proportions of Ki67+ (G), Pax6+ (H), βIII-tubulin+ (I) and CC3+ cells (J). Scale bar = 50
136 μm. *, $p < 0.001$; n = 3 embryos per genotype. (K-O) E13.5 cortical precursor cells from single
137 $Dhcr7^{+/+}$ or $Dhcr7^{-/-}$ embryos were cultured as primary neurosphere (K) and the number and
138 diameter of primary neurospheres were quantified 6 days later (L, M). Equal numbers of primary
139 neurospheres were then passaged, and the number and diameter of secondary neurospheres were
140 quantified 6 days later (N, O). Representative images of $Dhcr^{+/+}$ and $Dhcr7^{-/-}$ neurospheres are
141 shown as inserts in the left corner. *, $p < 0.001$; n = 3 embryos per genotype. Scale Bar = 100
142 μm.
143 **Figure 1-Figure Supplement 1.** Characterization of the pluripotency of SLOS-derived human
144 iPSCs.
145 **Figure 1-Figure Supplement 2.** Loss of *DHCR7* alleles causes decreased proliferation and
146 increased neurogenesis in human cortical precursors.
147

148
149 ***Loss of Dhcr7 Alleles Causes Decreased Proliferation and Increased Neurogenesis in Murine***
150 ***and Human Cortical Precursors***
151
152 SLOS is characterized by neurodevelopmental defects, such as microcephaly. To ask if
153 *Dhcr7* plays important roles in neural precursor (progenitor) development as seen in human
154 patients with SLOS, we intercrossed $Dhcr7^{+/-}$ mice and prepared single embryo cultures from
155 E12.5 $Dhcr7^{-/-}$ (knockout or KO) or $Dhcr7^{+/+}$ embryos. Cultures were immunostained for Ki67
156 and βIII-tubulin 3 days after plating, which revealed that loss of *Dhcr7* caused significant
157 decrease in the proportion of Ki67+ and Pax6+ precursors whereas increased the proportion of
158 βIII-tubulin+ neurons (Figure 1F-I). Immunostaining for cleaved caspase 3 (CC3) showed that
159 the loss of *Dhcr7* alleles did not affect the survival of cortical precursor cells in culture (Figure

160 1J). These results suggested that loss of *Dhcr7* leads to premature neurogenesis and decreased
161 proliferation of cortical precursors.

162 To determine if Dhcr7 is important for the proliferation and self-renewal of cortical
163 precursors, we performed neurosphere assays, which assess if sphere-forming precursors can
164 self-renew and generate new spheres. E13.5 cortical precursors from *Dhcr7*$^{-/-}$ and *Dhcr7*$^{+/+}$
165 embryos were cultured in the presence of FGF2 and EGF. The number and diameter of spheres
166 were measured 7 days post-plating (Figure 1K-O). Significantly fewer number of and smaller
167 neurospheres were generated from *Dhcr7*$^{-/-}$ embryonic cortices comparing to its wild-type
168 littermates (Figure 1L-M). These results were consistent with the reduced proportion of Ki67+
169 precursors in the adherent cultures. Following formation of the primary neurospheres, these
170 spheres were triturated and re-plated at equal density to form the secondary neurospheres. The
171 results showed that there was an approximately 2-fold decrease in the number and diameter of
172 secondary spheres from *Dhcr7*$^{-/-}$ cortical precursors relative to *Dhcr7*$^{+/+}$ (Figure 1N-O). Thus,
173 the loss of *Dhcr7* alleles disrupts proliferation and self-renewal of cortical precursors.

174 We then asked whether *DHCR7* was also necessary for neurogenesis of human
175 embryonic stem cell-derived NPCs. To examine function of DHCR7, we generated human
176 induced pluripotent stem cells (hiPSCs) from two lines of SLOS patient fibroblasts and one line
177 of wild-type fibroblasts and verified their pluripotency and stemness as described in Methods
178 (Figure 1-Figure Supplement 1) (Okita et al., 2011; Yu et al., 2007). The SLOS hiPSCs were
179 then differentiated into hNPCs as described previously. Immunoreactivity of DHCR7 was
180 detected in almost all wild-type hNPCs in these cultures with Sox2+ and Nestin+ cells (Figure 1-
181 Figure Supplement 2; Panel A). To examine neural differentiation, the SLOS and wild-type
182 NPCs were differentiated in cultures and immunostained 4 days later for Ki67 and βIII-tubulin

183 for proliferating precursors and newborn neurons, respectively (Figure 1-Figure Supplement 2;
184 Panels B-D). Notably, the proportion of Ki67+ precursors was significantly decreased whereas
185 the proportion of βIII-tubulin+ neurons was increased in SLOS NPC cultures, similar to the
186 phenotype seen in murine cortical precursors from *Dhcr7*$^{-/-}$ embryos. Taken together, DHCR7 is
187 involved in proliferation and differentiation of human NPCs.

188 ***Cholesterol precursor 7-DHC and 7-DHC-derived Oxysterols are accumulated in Dhcr7***$^{-/-}$
189 ***developing cortex and human NPCs***
190
191 7-DHC is highly susceptible to free radical oxidation (Xu et al., 2009), which leads to
192 formation of numerous oxysterols in cells and tissues (Xu et al., 2013; Xu et al., 2011) (Figure
193 2A). Liquid chromatography-tandem mass spectrometry (LC-MS/MS) was performed on
194 cortices from *Dhcr7*$^{-/-}$ and *Dhcr7*$^{+/+}$ embryos during cortical development. These analyses
195 revealed significant accumulation of 7-DHC and reduction of cholesterol in the embryonic
196 cortices from *Dhcr7*$^{-/-}$ embryos throughout cortical development from E12.5 to E16.5 (Figure
197 2B). Increased levels of 7-dehydrodesmosterol (7-DHD), the precursor to desmosterol via
198 Dhcr7, and 8-dehydrocholesterol (8-DHC) and decreased level of desmosterol in *Dhcr7*$^{-/-}$
199 cortices are also consistent with the loss of the function of Dhcr7. Furthermore, 7-DHC
200 oxysterols, such as DHCEO, 4α-hydroxy-7-DHC (4α-OH-7DHC), and 4β-hydroxy-7-DHC (4β-
201 OH-7DHC) (Xu et al., 2013; Xu et al., 2011) showed substantial accumulation in the *Dhcr7*$^{-/-}$
202 cortices, reaching up to 4-8 ng/mg of tissue, throughout the development (Figure 2A and 2C).
203 Note that 4 ng/mg of tissue would translate into approximately 10 μM assuming the density of
204 the brain is 1 g/mL. On the other hand, cholesterol-derived oxysterols, such as 24-keto-Chol,
205 24,25-epoxy-Chol, 24- or 25-OH-Chol, 7-OH-Chol, and 7-keto-Chol decreased or did not
206 change significantly in *Dhcr7*$^{-/-}$ cortices relative to *Dhcr7*$^{+/+}$ cortices.

207 Furthermore, significant accumulation of 7-DHC and 7-DHC-derived oxysterols and
208 reduction of cholesterol were also found in both SLOS patient-derived hiPSCs and NPCs relative
209 to wild type (Figure 2-Figure Supplement 1). Taken together, *DHCR7* mutations led to
210 accumulation of 7-DHC and 7-DHC-derived oxysterols in murine and human cortical precursors.

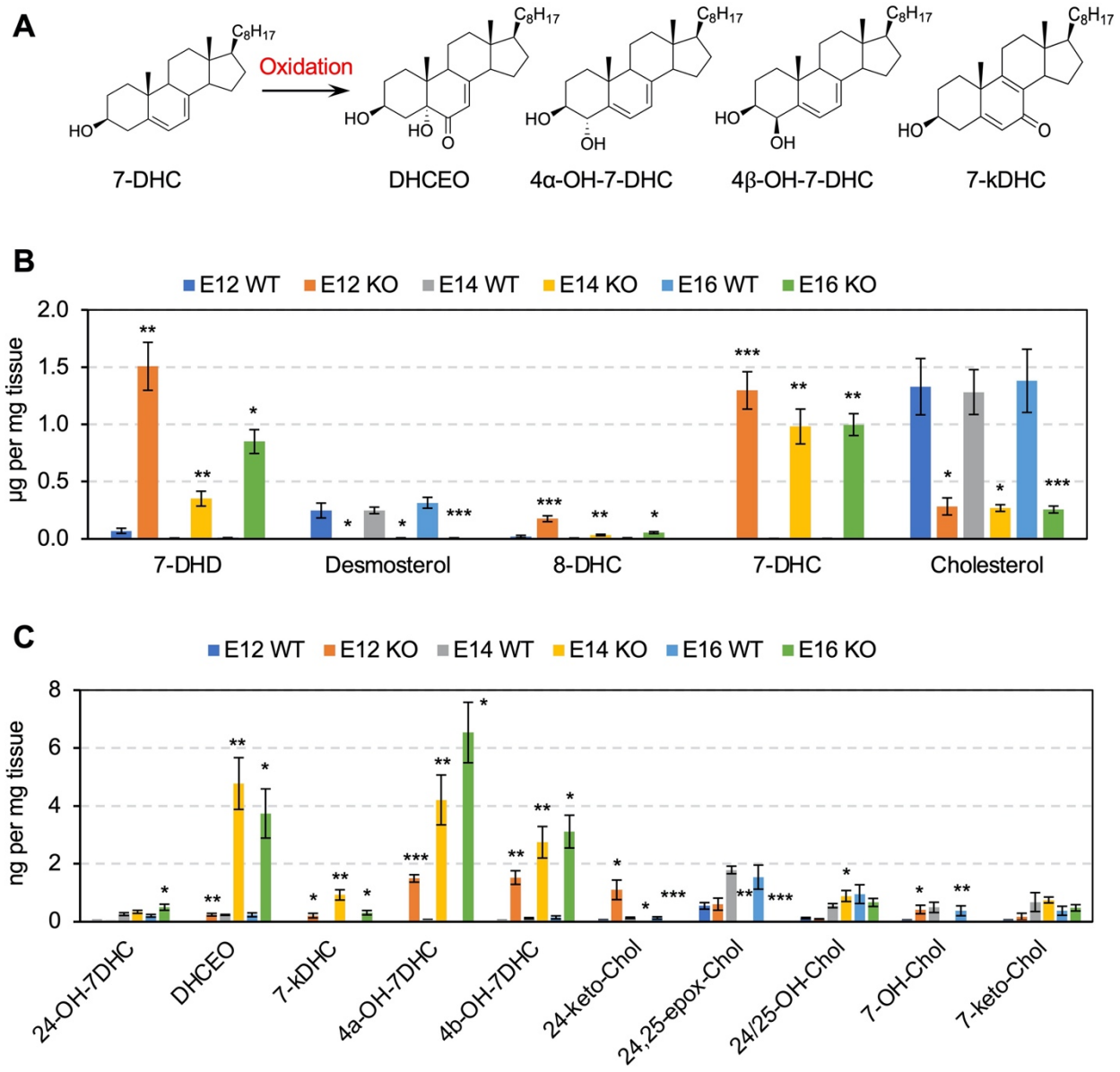

211
212 **Figure 2. Cholesterol precursor 7-DHC and 7-DHC-derived Oxysterols are accumulated in**
213 ***Dhcr7*$^{-/-}$ mouse embryonic cortex.** (A) Chemical structures of 7-DHC-derived oxysterols. LC-
214 MS/MS analysis of (B) cholesterol and its precursors and (C) 7-DHC-derived oxysterols in
215 *Dhcr7*$^{+/+}$ and *Dhcr7*$^{-/-}$ embryonic cortex during development. Error bars indicate standard
216 deviation. *, $p < 0.05$; **, $p < 0.005$; ***, $p < 0.001$; n = 3 biological replicates per group.

217 **Figure 2-Figure Supplement 1.** Cholesterol precursor 7-DHC and 7-DHC-derived Oxysterols
218 are accumulated *in* SLOS-derived human iPSCs and NPCs.
219

220 ***Knockdown (KD) of Dhcr7 Causes Increased Neurogenesis and Depletion of Cycling***
221 ***Precursors in Murine and Human NPC cultures***
222
223 To examine a potential role of *Dhcr7*, we generated three *Dhcr7* short hairpin RNAs
224 (shRNAs)-EGFP reporters and transfected them into 293T cells along with murine *Dhcr7*
225 cDNA-expressing plasmids. We found that *Dhcr7* shRNA2 was the most effective among those
226 shRNAs and was chosen to examine *Dhcr7* function during neurogenesis from E12.5 cortical
227 precursors in culture (Figure 3A). When cortical precursors were transfected with *Dhcr7*
228 shRNA2-EGFP, the shRNA significantly decreased the percentage of transfected cells
229 expressing *Dhcr7* (Figure 3B-C). *Dhcr7* KD led to a significant decrease in proliferation of
230 cortical precursors as measured by Ki67 immunostaining and significant increase of βIII-
231 tubulin+ neurons 3 days post-transfection, but it did not affect cell survival as examined by
232 immunostaining for CC3 (Figure 3D-G). The significant decrease of precursor proliferation was
233 caused by a decrease in Pax6+ radial precursors (Figure 3H).
234 *Dhcr7* KD also decreased self-renewal of radial precursor as demonstrated by clonal
235 analysis with piggybac (PB) transposon, which permanently labels precursors and their progeny.
236 Cortical precursors were transfected with PB transposase and PB-*Dhcr7* shRNA2-EGFP or
237 control shRNA-EGFP, and cultures were immunostained 3 days post-transfection for EGFP, the
238 precursor markers, Sox2, and βIII-tubulin (Figure 3I-L). KD of *Dhcr7* reduced EGFP+
239 multicellular clones (Figure 3J) whereas neuron-only (βIII-tubulin+) clones were increased
240 (Figure 3K). Furthermore, the number of precursors in clones containing at least one Sox2+
241 cells are decreased (Figure 3L).

242 To ensure that these changes were *Dhcr7* shRNA-dependent, we performed a rescue
243 experiments using human *DHCR7* cDNA that is resistant to the murine *Dhcr7* shRNA (Figure 3-
244 Figure Supplement 1). The murine shRNA did not affect the expression of human DHCR7
245 cDNA as confirmed by co-transfection of the murine shRNA and human *DHCR7* cDNA in 293T
246 cells and western blot analysis 2 days later (Figure 3-Figure Supplement 1; Panel A).
247 Furthermore, precursors were co-transfected with murine *Dhcr7* shRNA-EGFP or control
248 shRNA-EGFP +/- human *DHCR7* cDNA and immunostained 3 days later for Ki67 or βIII-
249 tubulin (Figure 3-Figure Supplement 1). The human *DHCR7* cDNA showed significant rescue
250 of the murine *Dhcr7* shRNA KD phenotypes, confirming the specificity of the shRNA.

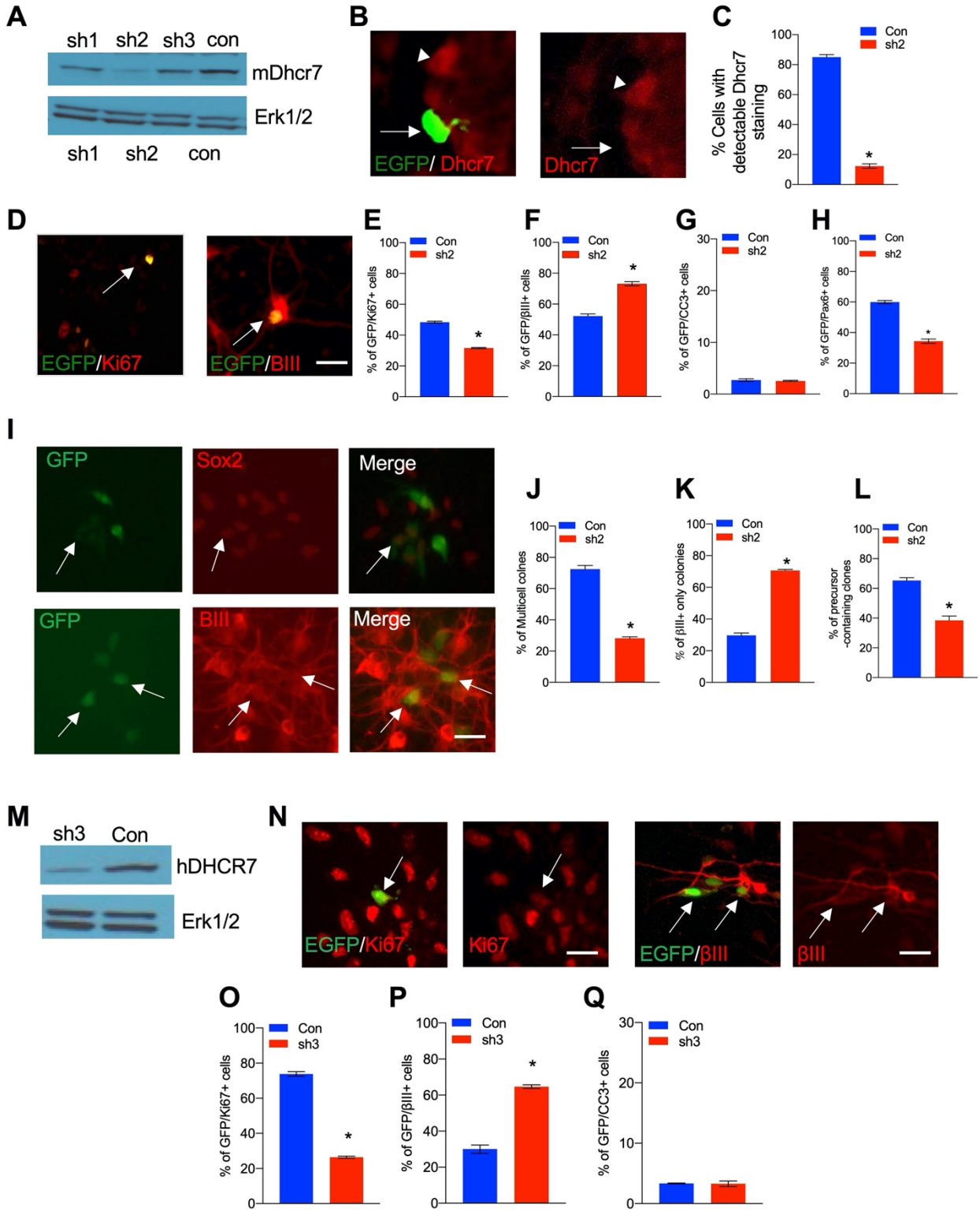

Figure 3. Knockdown of *Dhcr7* causes increased neurogenesis and depletion of cycling precursors in murine and human NPC cultures. (A) Western blot for Dhcr7 in 293T cells transfected with control or individual murine *Dhcr7* shRNAs. The blot was re-probed for Erk1/2 as a loading control. (B and C) Mouse cortical precursors were transfected EGFP-*Dhcr7* shRNAs (sh2) or EGFP-control (Con) and immunostained for EGFP and Dhcr7 (red) 2 days later

257 and EGFP+ cells expressing detectable Dhcr7 were quantified by fluorescence intensity (C).
258 Arrow and arrowhead in (B) denote EGFP+/Dhcr7- and EGFP-/Dhcr7+ cells, respectively. (D-
259 G) E12.5 cortical precursors were transfected with control or *Dhcr7* shRNAs and analyzed 3
260 days later. (D) Cultures were immunostained for EGFP (green) and Ki67 or βIII-tubulin (red;
261 double-labelled cells in orange are indicated with arrows) or CC3 and the proportion of total
262 EGFP+ cells that were also positive for Ki67 (E), βIII-tubulin (F) or CC3 (G) was quantified. *,
263 $p < 0.001$; n = 3. Scale bar = 50 μm. In all cases, error bars denote SEM. **(**H-K) E12.5
264 precursors were co-transfected with the PB transposase and PB-EGFP-control (Con) or PB-
265 EGFP-*DHCR7* shRNA (sh2). (H) Cultured cells were immunostained for EGFP (green), Sox2
266 (red) and βIII-tubulin (red) after 3 days and quantified for clones greater than one cell in size (I),
267 neuron-only clones (J), and clones with at least one Sox2+ precursors (K). Arrows in (I) top
268 denote EFGP+/ Sox2+ precursors. Arrow in (I) bottom denote EGFP+/βIII-tubulin+ cells. *, $p <$
269 0.001; n = 3. (M) Western blots of DHCR7 in 293T cells transfected with human control (Con)
270 or human-specific *DHCR7* shRNA (sh3) plus human *DHCR7*-expressing plasmid, analyzed after
271 24 hr. The blot was re-probed for Erk1/2. (N) Human cortical precursors were transfected with
272 EGFP-control (Con) or EGFP-*DHCR7* shRNA (sh3). Cells were immunostained 3 days later for
273 EGFP (green) and Ki67 (red), βIII-tubulin (red) or CC3 and the proportion of total EGFP+ cells
274 that were also positive for Ki67 (O), βIII-tubulin (P), or CC3 (Q) was quantified. *, $p < 0.001$; n
275 = 3. Scale Bar = 50 μm. Allows in (N) denote double-positive cells.
276 **Figure 3-Figure Supplement 1.** Rescue of the neurogenesis phenotype in *Dhcr7*-knockdown
277 mouse cortical precursors by human *DHCR7* cDNA expression vector.
278

279 Finally, we asked whether *Dhcr7* also plays a role in human iPSC-derived NPCs (Figure
280 3M-Q). To examine the function of DHCR7, we generated a human-targeted *DHCR7* shRNA-
281 EGFP and confirmed its efficiency by transfecting it into 293T cells along with human DHCR7
282 expressing vectors (Figure 3M). Human NPCs were transfected with this shRNA-EGFP and
283 analyzed by immunostaining 4 days later, which showed that the KD of human *DHCR7* reduced
284 EGFP+ and Ki67+ proliferating precursors whereas increased EGFP+ and βIII-tubulin+ newborn
285 neurons (Figure 3N-Q), similar to those observed in murine cortical precursors and SLOS
286 hNPCs.

287
288 ***7-DHC Derived Oxysterols Lead to Similar Neurogenic Defects as loss of Dhcr7 in Murine***
289 ***Cortical precursors in vitro***
290
291 Oxysterols have been found to influence biological processes, including proliferation,
292 differentiation and cell survival (DuSell et al., 2008; Theofilopoulos et al., 2013; Voisin et al.,

293 2017). Thus, we asked whether 7-DHC-derived oxysterols play regulatory roles in cortical
294 precursor biology. To assess potential effect of these 7-DHC-derived oxysterols on cortical
295 precursor behaviors, cortical precursors from E12.5 wild-type embryos were cultured and treated
296 with different concentrations of individual oxysterols for 3 days, followed by immunostaining
297 for Ki67, βIII-tubulin, and CC3 (Figure 4A). Notably, DHCEO-treated cortical precursor
298 showed significant increase in the proportion of βIII-tubulin+ newborn neurons and significant
299 decrease in the proportion of Ki67+ precursors (Figure 4B-C). This effect of DHCEO was
300 observed in a dose-dependent manner up to 3.5 μM, which is roughly the concentration of
301 DHCEO in the brains of P0 *Dhcr7*-KO mice (Xu et al., 2011). There was no significant change
302 in cell death/survival with DHCEO treatment (Figure 4D). The other oxysterols showed notable
303 toxic effect at a concentration of 5 μM as indicated by increased CC3+ cells (Figure 4G, 4J, and
304 4M). Note that the level of 7k-DHC is the lowest among the oxysterols, only reaching 0.9 ng/mg
305 of tissue (equivalent to 2.3 μM), so we do not expect the highest concentration examined, 5 μM,
306 for this oxysterol is relevant to the neurogenic phenotype. Interestingly, 4α-OH-7DHC treatment
307 at a concentration of 2 μM also displayed significant increases in βIII-tubulin+ neurons and
308 decreases in Ki67+ precursors without significant changes in cell death/survival (Figure 4H-J).
309 However, at 5 μM, CC3+ cells were significantly elevated at the expense of βIII-tubulin+
310 neurons (Figure 4J). To summarize, treatment with DHCEO at physiologically relevant
311 concentrations completely replicated the premature neurogenic phenotype observed in murine
312 and human SLOS NPCs while 4α-OH-7DHC may also contribute to the phenotype despite its
313 toxicity at high concentration.

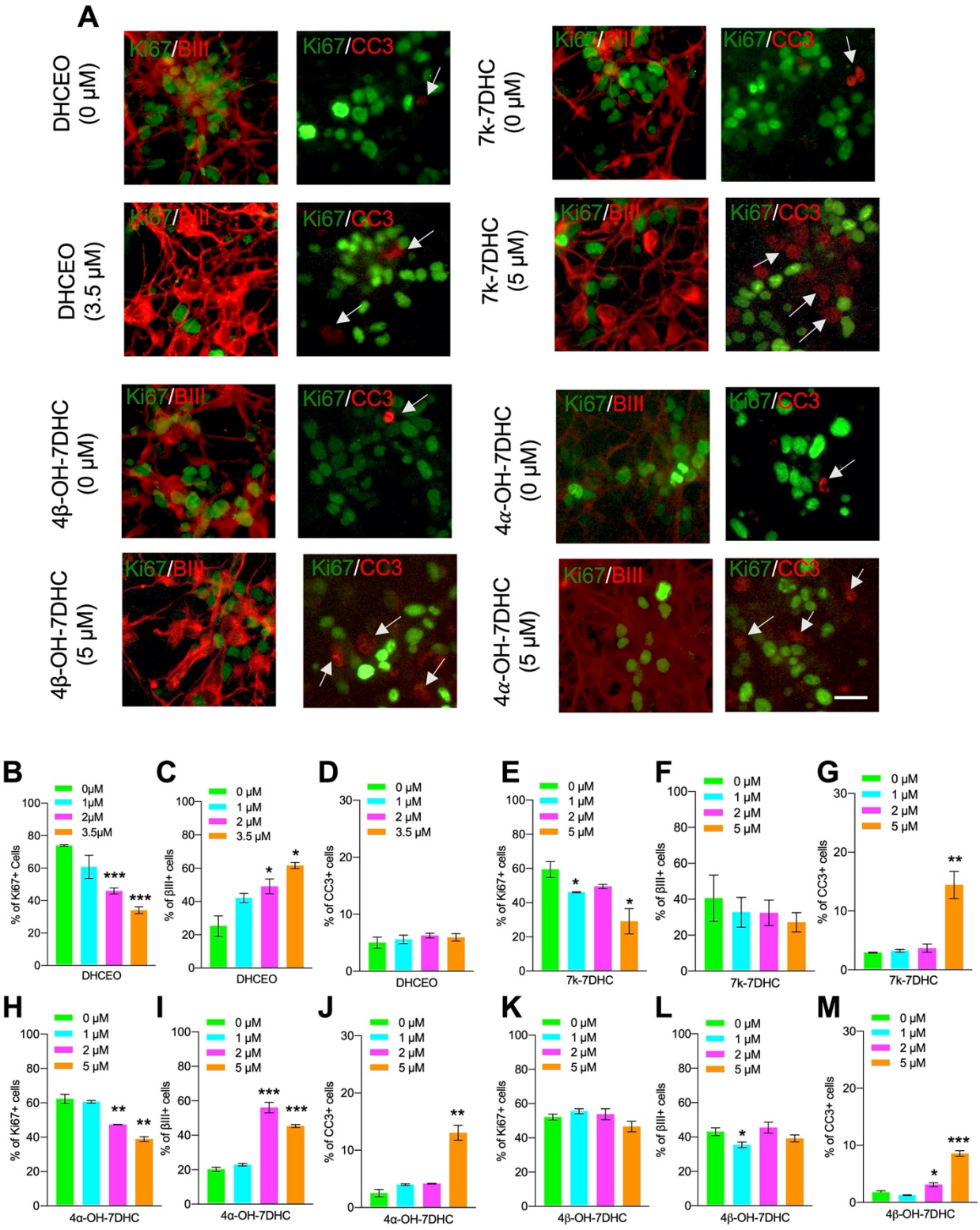

Figure 4. 7-DHC Derived Oxysterols Lead to Similar Neurogenic Defects as loss of *Dhcr7* in Murine Cortical precursors *in vitro*. (A-M) E12.5 cortical precursors were cultured for 2 days in the presence of different concentrations of 7-DHC-derived oxysterols and quantified.

(A) Cell were immunostained for Ki67 (green), βIII-tubulin (red), and CC3 (red, arrow) after 3 days and the proportions of Ki67+ (B,E,H,K), βIII-tubulin+ (C,F,I,L), and CC3+ (D,G,J,M) cells were determined. Error bars indicate SEM. *, $p < 0.05$; **, $p < 0.005$; ***, $p < 0.001$. n = 3 per experiment. Scale Bar = 50 µm.

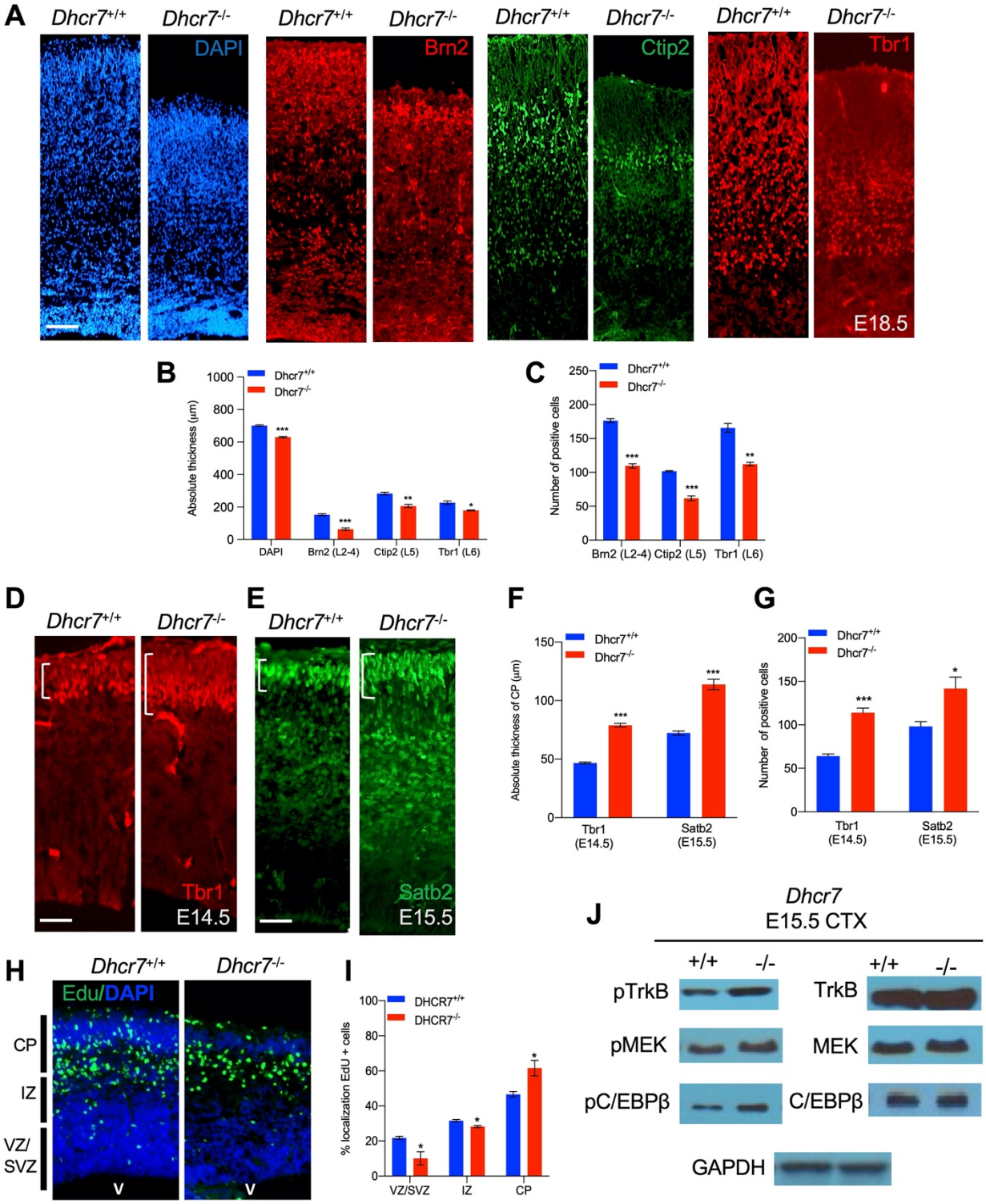

325 **Figure 5. *Dhcr7*$^{-/-}$ mice display premature neurogenesis, altered neocortical**
326 **cytoarchitecture *in vivo*, and increased activity of TrkB neurogenic signaling pathway.** (A)
327 E18.5 cortical sections from *Dhcr7*$^{+/+}$ and *Dhcr7*$^{-/-}$ were immunostained for Tbr1 (red), Ctip2
328 (green) and counterstained with DAPI (blue). (B and C) Quantifications of absolute thickness
329 (B) and number of positive cells (C). (D-G) Cortical sections from E15.5 *Dhcr7*$^{+/+}$ and *Dhcr7*$^{-/-}$
330 mice were immunostained for Satb2 (D, green) and Tbr1 (E, red). Quantifications of absolute
331 thickness (F) and number of positive cells (G) for Satb2 and Tbr1. (H) E15.5 cortical sections
332 from *Dhcr7*$^{+/+}$ and *Dhcr7*$^{-/-}$ embryos EdU-labeled at E12.5 were immunostained for EdU (green)
333 and counterstained with DAPI (blue). (I) Quantification of relative location of EdU+ cells in
334 cortical sections. (J) E15.5 cortices were isolated from *Dhcr7*$^{+/+}$ and *Dhcr7*$^{-/-}$ embryos and
335 analyzed by western blot for phospho-TrkB, phospho-MEK, or phospho-C/EBPβ. Blots were re-
336 probed with antibodies for total GR, TrkB, MEK, C/EBPβ and GAPDH as loading controls.
337 Error bars indicate SEM. *, $p < 0.05$; **, $p < 0.005$; ***, $p < 0.001$. n = 3 per experiment. Scale
338 Bar = 50 μm.
339
340

341 ***Loss of Dhcr7 causes premature differentiation and alter neocortical cytoarchitecture in vivo***
342
343 We asked whether loss of *Dhcr7* disrupted cortical development *in vivo* as was observed
344 *in vitro*. To examine this, cortical sections from *Dhcr7*$^{-/-}$ mice at E18.5 were immunostained for
345 the expression of well-defined cortical layer markers: the layer 2-4 marker Brn2, the layer 5
346 marker CTIP2, and the layer 6 marker Tbr1 (Molyneaux et al., 2007) (Figure 5A). The analyses
347 showed loss of *Dhcr7* led to reduction of all cortical layers, resulting in reduction of overall size
348 of the neocortex (Figure 5B-C). To further evaluate the effects of *Dhcr7* mutations in fate
349 decision of cortical precursors during corticogenesis, we immunostained cortical sections from
350 *Dhcr7*$^{-/-}$ mice at E14.5 and E15.5 for Tbr1 and Satb2, which label early-born and late-born
351 cortical neurons, respectively (Figure 5D-E). The analyses showed the significant increase of
352 Tbr1+ neurons and Satb2+ neurons in cortical section from *Dhcr7*$^{-/-}$ mice at E14.5 and E15.5,
353 respectively (Figure 5F-G). This aberrant increased production of neurons with loss of *Dhcr7*
354 potentially hinders proper localization of developing neurons in the cortex. To test this
355 hypothesis, we injected pregnant dams with 5-ethynyl-2-deoxyuridine (Edu) at E12.5 to label
356 proliferating radial precursors and analyzed *Dhcr7*$^{+/+}$ and *Dhcr7*$^{-/-}$ littermates three days later at

357 E15.5 to identify the locations of Edu-labeled cells in the cortex (Figure 5H-I). Majority of Edu-
358 labeled cells migrated into the cortical plate in the KO mice whereas Edu-labeled cells were
359 scattered throughout the intermediate zone (IZ) and the cortical plates in the wild-type
360 littermates. These observations suggest premature increases in precursor differentiation, which
361 raises the possibility of activating major neurogenic signaling pathways during corticogenesis.
362 RTKs and their downstream targets are known to play important roles in precursor proliferation
363 and differentiation in developing cortex, and TrkB, one of the major RTKs expressed in cortical
364 precursors, regulates proliferation and differentiation into neurons by activating the MEK-ERK-
365 C/EBP pathway (Barnabe-Heider and Miller, 2003; Bartkowska et al., 2007; Menard et al.,
366 2002). Thus, we examined the activity of TrkB-MEK-ERK-C/EBP pathway by western blot with
367 antibodies for phosphorylated activated MEK1 and C/EBPβ at E15.5 of *Dhcr7*$^{-/-}$ cortices (Figure
368 5J). This analysis showed that relative to total MEK1 and ERK1/2 levels, their phosphorylated
369 forms increased in *Dhcr7*$^{-/-}$ cortices. This observation suggests that loss of *Dhcr7* can
370 dysregulate an RTK-dependent signaling pathway that is critical for neural precursor
371 proliferation and differentiation.

372 The above observations indicate premature precursor differentiation at the expense of
373 depleting the proliferative precursor pool. To examine this hypothesis, pregnant dams were
374 injected with Edu at different time points of cortical development, and *Dhcr7*$^{+/+}$ and *Dhcr7*$^{-/-}$
375 littermates were analyzed 18 hours later to quantify the number of cycling progenitors that have
376 exited the cell cycles (Figure 6A-B). Cells that had left the cell cycle were stained as Edu+ and
377 Ki67- whereas cells that re-entered the cell cycle were stained as Edu+ and Ki67+. The index of
378 the cell cycle exit is defined by the percentage of Edu+/Ki67- cells in total Edu+ cells. The
379 index showed that the number of cells exiting the cell cycle in *Dhcr7*$^{-/-}$ cortices was significantly

380 increased at E13.5 and E14.5 compared with *Dhcr7*$^{+/+}$ cortices, indicating that loss of *Dhcr7*
381 increased cell cycle exit. Increased cell cycle exit of cortical precursors can potentially arise from
382 changes in proliferation. To test this possibility, pregnant dams were pulsed with Edu for 2 hours
383 to label all cells in S-phase and the fraction of cortical precursors in S-phase, a proliferating
384 index from E13.5 to E15.5 in *Dhcr7*$^{-/-}$ and *Dhcr7*$^{+/+}$ cortices, was quantified (Figure 6C-D). The
385 proliferating index was determined by the percentage of Edu+ and Ki67+ cells out of total Ki67+
386 cells, which provides an estimate of cell cycle length because the length of S phase remains
387 relatively constant in mammalian cells, whereas the length of G1 phase regulates proliferation
388 (DiSalvo et al., 1995). The analyses showed a significant decrease in the proliferating index in
389 *Dhcr7*$^{-/-}$ cortices compared to *Dhcr7*$^{+/+}$ cortices from E13.5 to E15.5 (Figure 6C-D), indicating
390 slower cycle progression and longer cycle length in *Dhcr7*$^{-/-}$ cortices (Chenn and Walsh, 2002).
391 Indeed, this accelerated depletion of the progenitor pool in *Dhcr7*$^{-/-}$ cortices result in decreases in
392 the size of VZ/SVZ compared to *Dhcr7*$^{+/+}$ cortices from E13.5 to E15.5 (Figure 6E-F). Taken
393 together, these results suggest that loss of *Dhcr7* leads to a decrease in the overall number of
394 cortical precursors with increased cell cycle exit and decreased proliferation index via activation
395 of RTK-mediated MEK-ERK-C/EBP pathway.

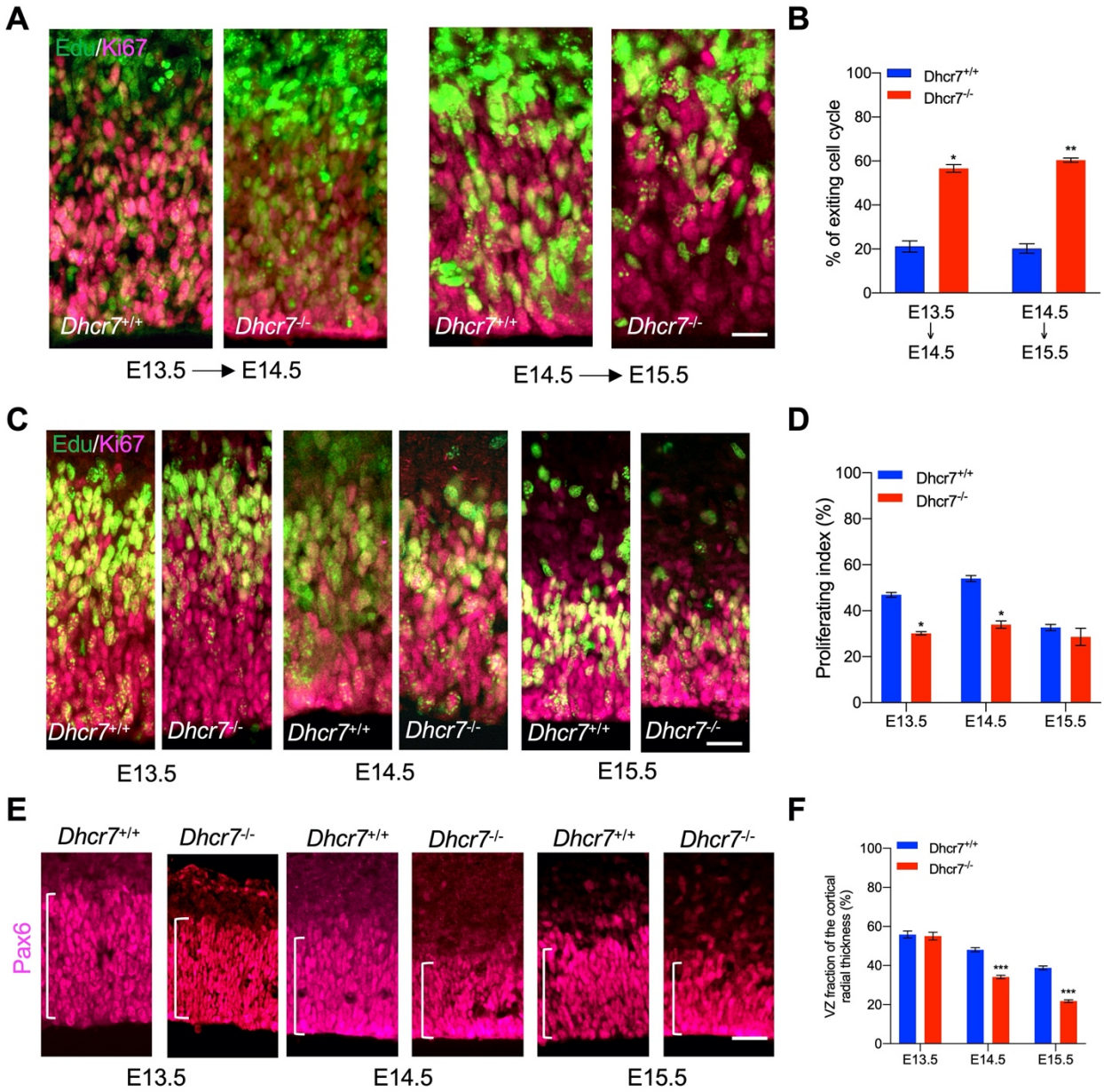

Figure 6. *Dhcr7*$^{-/-}$ mice show accelerated cell cycle exiting and depletion of cortical precursor cells *in vivo*. (A) Cortical sections from *Dhcr7*$^{-/-}$ and *Dhcr7*$^{+/+}$ embryos labeled by Edu at different developmental stages were immunostained 18 hours later for Edu (green) and Ki67 (Magenta). (B) Quantification of cell-cycle exit index of *Dhcr7*$^{-/-}$ cortices compared with *Dhcr7*$^{+/+}$ cortices. (C) Cortical sections from *Dhcr7*$^{-/-}$ and *Dhcr7*$^{+/+}$ embryos labeled by Edu injection at different developmental stages were immunostained 2 hours later for Edu (green) and Ki67 (Magenta). (D) Quantification of proliferation index of *Dhcr7*$^{-/-}$ cortices compared with *Dhcr7*$^{+/+}$ cortices. (E) Coronal cortical sections immunostained for Pax6 cortical precursor marker at different developmental stages. (F) Quantification of the relative size of the Pax6+ region shown as fractions of the whole cortical radial thickness. Error bars indicate SEM. *, $p < 0.05$; **, $p < 0.005$; ***, $p < 0.001$. n = 3 per experiment. Scale Bar = 50 μm.

410 ***Perturbation in DHCR7 Causes Gene Expression Changes in Neurogenic Pathways in***
411 ***Human NPCs***
412
413 To ask whether *DHCR7* mutations influence the NPC biology, we aim to compare gene
414 expression profiles between hNPCs with *DHCR7* mutations versus hNPCs from healthy
415 individuals. To do so, we expanded the hNPCs derived from hiPSCs in the presence of essential
416 growth factors and carried out RNA sequencing (RNAseq) on these cells. Relative to wild-type
417 hNPCs, 2357 genes were significantly differentially expressed in SLOS hNPCs (1072
418 upregulated and 1285 downregulated genes with adjusted p value < 0.05), distinguishing the
419 SLOS and wild-type precursors (Figure S1A; Table S6 for RNAseq data). Gene ontology and
420 pathway analysis found that PI3K-Akt signaling pathway, MAPK signaling, and Ras signaling
421 pathways are among those with the highest p-values (Figure S1B-C; Table S5). Notably,
422 MAP2K1(also known as MEK1) was found to be upregulated in SLOS patient-derived hNPCs.
423 MAP2K1 is a key signaling molecule in MAPK and Ras signaling pathways, which are known to
424 play important roles in precursor proliferation and differentiation (Bonni et al., 1999; Menard et
425 al., 2002; Yang et al., 2013), consistent with the phenotypes that were observed in *Dhcr7*-KO
426 mice and SLOS patient-derived hNPCs *in vitro*.

427 ***7-DHC-derived oxysterol, DHCEO, activates cortical neurogenesis via activation of***
428 ***glucocorticoid receptor and inhibition of GR or inhibition of the formation of DHCEO rescues***
429 ***the neurogenic defects in SLOS NPCs***
430
431 As shown in Figure 4, treatment of WT mouse NPCs with 7-DHC-derived oxysterols,
432 particularly DHCEO, can replicate the same aberrant premature neurogenesis observed in SLOS
433 NPCs. However, the mechanism of action of DHCEO remains unknown. Interestingly, 6-oxo-
434 cholestan-3β,5α-diol (OCDO), a cholesterol-derived oxysterol that is structurally similar to
435 DHCEO, is shown to bind and activate glucocorticoid receptor (GR) (Voisin et al., 2017) (Figure
436 7-Figure Supplement 1; Panel A). Additionally, GR activation is shown to activate TrkB

437 (Jeanneteau et al., 2008), which leads to further activation of RTK-mediated MEK-ERK pathway
438 (Barnabe-Heider and Miller, 2003; Bartkowska et al., 2007; Menard et al., 2002). TrkB and
439 RTK-mediated MEK-ERK pathway are necessary for neurogenesis during embryonic cortical
440 development. Thus, we asked whether DHCEO can activate the GR and further lead to the
441 activation of MEK-ERK neurogenic pathway. To investigate this, we first examined if GR was
442 phosphorylated and activated in the embryonic cortices from *Dhcr7*$^{-/-}$ and *Dhcr7*$^{+/+}$ embryos at
443 E15.5 in addition to TrkB, MEK, and C/EBPβ shown in Figure 5J. Western blots demonstrated
444 that phosphorylation of GR was indeed increased in *Dhcr7*$^{-/-}$ cortices comparing to *Dhcr7*$^{+/+}$
445 cortices (Figure 7A).

446 To ask if DHCEO could physically interact with GR, we performed molecular docking
447 simulation between DHCEO and the ligand binding domain of GR. Molecular docking is an
448 effective computational approach to understand protein-ligand interaction between small
449 molecules and receptor proteins both energetically and geometrically (Ferreira et al., 2015). As
450 seen in Figure 7B, DHCEO docks in the binding pocket of human GR favorably with a docking
451 score of -9 (a negative value suggests favorable interactions), comparable to the docking score of
452 OCDO at -9.5.

453 We further examined whether DHCEO could initiate GR and TrkB activation in wild-
454 type hNPCs *in vitro*. Cultured hNPCs were exposed to DHCEO (3.5 μM), a physiologically
455 relevant concentration, harvested at the different time points (3, 6, 9 and 24 hrs), and evaluated
456 for GR and TrkB activation by western blots (Figure 7C), which revealed that DHCEO-treated
457 hNPCs showed a gradual increase of phosphorylated GR starting at 3 hrs and peaking at 10 hrs
458 of exposure. As GR phosphorylation increased, DHCEO-treated hNPCs also showed the
459 phosphorylation of TrkB from 6 hrs to 10 hrs exposure, which dissipated at 24hrs exposure. As

460 no exogenous GR ligands and neurotrophins were added in these experiments, these results

461 indicated that DHCEO caused the increased phosphorylation of GR, which led to the activation

462 of TrkB phosphorylation in human NPCs *in vitro*.

463

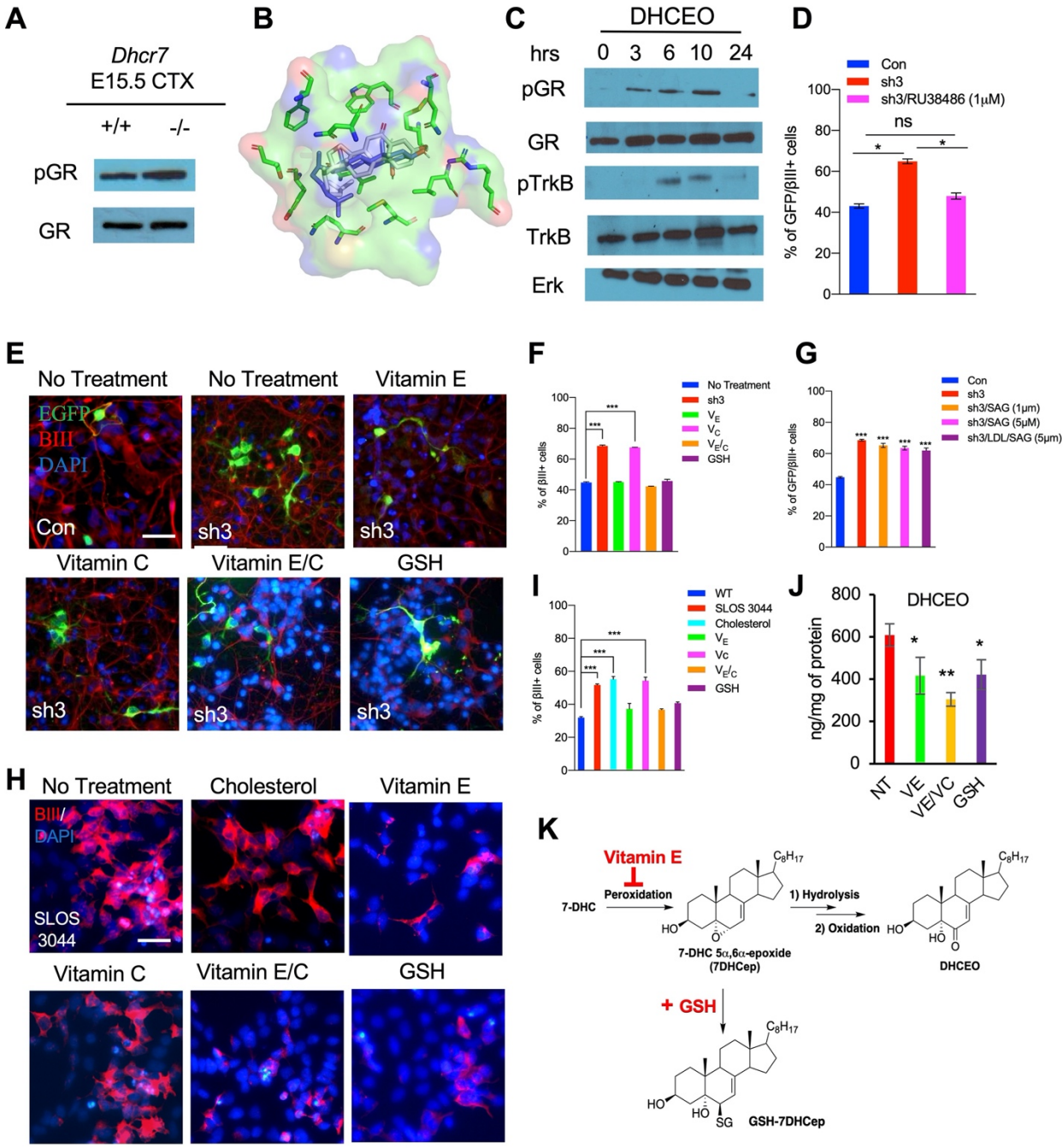

464

465 **Figure 7. DHCEO activates cortical neurogenesis via activation of glucocorticoid receptor**
466 **and inhibition of the effect or the formation of DHCEO rescues the neurogenic defects in**

467 **SLOS NPCs.** (A) Western blot showing increased phospho-GR in E15.5 *Dhcr7*$^{-/-}$ mouse brain
468 relative to *Dhcr7*$^{+/+}$. (B) Image of the docked position of DHCEO (white) and OCDO (blue) in
469 the ligand binding pocket of GR. (C) Human neural progenitors were treated with 3.5 μM
470 DHCEO over the indicated time periods. Lysates were probed with phosphor-GR and phosphor-
471 TrkB and re-probed with antibodies for total GR, total TrkB or total ERK as loading controls.
472 (D) Human NPCs were transfected with EGFP-control (Con) or EGFP-*DHCR7* (sh3) shRNA.
473 Cells were treated with 1 μM RU38486, a selective GR antagonist one day after transfection.
474 Three days post-transfection, cells were immunostained for EGFP and βIII-tubulin and
475 quantified. (E) Wild type hNPCs were transfected with EGFP-control (Con) or EGFP-*DHCR7*
476 shRNA (sh3), and then treated with vitamin E, vitamin C, vitamin E/C, or glutathione (GSH).
477 Three days post-transfection, cells were immunostained for EGFP and βIII-tubulin. (F,G)
478 Quantification of EGFP and βIII-tubulin+ cells in *DHCR7*-KD wild-type hNPCs treated with
479 various antioxidants, SAG, or LDL+SAG. (H) SLOS hNPCs were treated with cholesterol or
480 various antioxidants and were immunostained for βIII-tubulin and DAPI. (I) Quantification of
481 the proportion of βIII-tubulin+ cells in wild type hNPCs, and SLOS hNPCs treated with
482 cholesterol or various antioxidants. (J) Quantification of DHCEO by LC-MS/MS in SLOS
483 hiPSCs treated with vitamin E, vitamin E/C, and GSH. (K) Proposed mechanisms of actions of
484 vitamin E and GSH during free radical oxidation of 7-DHC. Error bars indicate SEM. *, $p <$
485 0.05; **, $p < 0.005$; ***, $p < 0.001$. n = 3 per experiment. Scale Bar = 50 μm.
486 **Figure 7-Figure Supplement 1.** Antioxidants rescue the neurogenic phenotype in human and
487 murine NPCs with *Dhcr7* mutations.
488

489 To confirm that GR activation could cause aberrant premature neurogenesis, we cultured
490 human cortical precursors and transfected them with *hDHCR7* shRNA-EGFP and control
491 shRNA-EGFP. 12 hours post-transfection, a glucocorticoid receptor antagonist, RU38486, or
492 vehicle control was added and cultured for 3 days. Cultures were immunostained for EGFP and
493 βIII-tubulin to evaluate the effects on neurogenesis. The analysis showed that inhibition of GR
494 by RU38486 rescued the *DHCR7*-KD-mediated increase in neurogenesis down to the level
495 observed in the control shRNA (Figure 7D).

496 Finally, we assessed whether aberrant premature neurogenesis was due to DHCEO, as it
497 is a major oxysterol derived from free radical (non-enzymatic) oxidation of 7-DHC (Xu et al.,
498 2011) (Figure 2). Antioxidants can prevent or slow down formation of oxysterols via the free
499 radical mechanism and protect cells from deleterious effects of oxysterols (Yin et al., 2011). In
500 particular, vitamin E (V_E), but not vitamin C (V_C), has been shown to effectively inhibit

501 formation of 7-DHC derived oxysterols in SLOS patient-derived fibroblasts (Korade et al.,
502 2014). Combination with V_C, which recycle oxidized V_E, enhances the antioxidant activity of V_E
503 against lipid peroxidation (Doba et al., 1985). Furthermore, glutathione (GSH) is an important
504 detoxifying molecule that is abundant (in mM) in cells and can potentially inhibit the formation
505 of DHCEO by reacting with its electrophilic precursor, 7-DHC 5α,6α-epoxide (Porter et al.,
506 2020; Xu et al., 2011). To test this possibility, we treated *hDHCR7* KD human cortical
507 precursors with antioxidants (V_E, V_C, V_E/V_C, or GSH) and then immunostained for EGFP and
508 βIII-tubulin to evaluate the effects on neurogenesis (Figure 7E-F). The analysis indicated that
509 V_E, V_E/V_C, or GSH, but not V_C alone, effectively reversed increased neurogenesis caused by
510 *hDHCR7* KD to the level observed in the control. Potential detoxifying effects of these
511 antioxidants were further tested in human SLOS patient-derived NPCs as well as cortical
512 precursors from *Dhcr7*$^{-/-}$ mouse embryos *in vitro* (Figure 7H-I and Figure 7-Figure Supplement
513 1, panels B-E). Treatments with V_E, V_E/ V_C and GSH were again found to effectively reduce the
514 increased neurogenesis in both human and murine cortical precursors with *Dhcr7* mutations
515 down to the level observed in WT samples. LC-MS/MS analysis confirmed that V_E, V_E/V_C, or
516 GSH indeed inhibited the levels of DHCEO in SLOS hiPSCs (Figure 7J). These results suggest
517 that free radical chain-breaking antioxidant, such as V_E, and nucleophilic antioxidant, such as
518 GSH, can effectively rescue the neurogenesis phenotype observed in SLOS NPCs by inhibiting
519 the free radical oxidation of 7-DHC at different stages (Figure 7K).
520 In addition to antioxidant treatment, we tested whether restoration of cholesterol could
521 potentially rescue aberrant premature neurogenesis observed in both human and murine SLOS
522 NPCs (Figure 7I, S6C and S6E). Low-density lipoprotein was added to cultures to examine the
523 effects of cholesterol on neurogenesis. The results revealed that addition of cholesterol did not

524 prevent increased neurogenesis in SLOS NPCs. Because DHCEO has been shown to inhibit
525 Smo in the Hh signaling pathway (Sever et al., 2016), we also tested whether supplementation of
526 SAG (a Smo agonist) can rescue the phenotype with or without cholesterol supplementation in
527 *DHCR7*-KD hNPCs (Figure 7G). However, none rescued the neurogenesis phenotype. Thus, the
528 lack of cholesterol and inhibition of Hh signaling do not contribute to the neurogenesis
529 phenotype observed in SLOS NPCs.

530 Taken together, the abnormal premature neurogenesis in cortical precursor with *Dhcr7*
531 mutations was caused by DHCEO activation of GR and further activation of Trk-mediated
532 neurogenic signaling pathway, but not by the deficiency in cholesterol, and inhibition of the
533 formation of DHCEO or GR rescues the neurogenic defects.

534

535 **Discussion**

536 Whether deficiency in cholesterol, accumulation of 7-DHC, or accumulation of 7-DHC
537 oxysterols is more important for the neurological and developmental phenotypes observed in
538 patients in SLOS remains unknown. Here, we characterized the neurogenic phenotype of SLOS
539 cortical precursors *in vitro* and *in vivo* and showed that the accumulated 7-DHC-derived
540 oxysterols, particularly DHCEO, disrupts normal embryonic neurogenesis by accelerating
541 progressive depletion of cortical precursors through neurogenesis, ultimately resulting in greatly
542 reduced cerebral cortex thickness with abnormal cortical layering.

543 The data presented here support four major conclusions. First, LC-MS/MS analyses
544 indicate that *DHCR7* mutations promote significant accumulation of 7-DHC-derived oxysterols
545 in murine and human embryonic cortical NPCs during cortical development. Second, our studies
546 with KD or KO of *DHCR7* indicate that *DHCR7* is necessary for normal proliferation of

547 embryonic NPCs and genesis of newborn neurons in culture and within the environment of the
548 embryonic cortex. KD or KO of *DHCR7* leads to premature differentiation of cortical precursors
549 to neurons and ultimately a perturbation in cortical cytoarchitecture. This occurs through the
550 activation of neurogenic TrkB-MEK-C/EBP pathway. Third, we show that 7-DHC-derived
551 oxysterols, especially DHCEO, display detrimental effects to normal neural development, and
552 that DHCEO can activate GR, which is responsible for abnormal cortical precursor
553 differentiation, since *DHCR7* KD/KO phenotype can be rescued by concurrent inhibition of
554 glucocorticoid receptor. Fourth, we show that premature differentiation of cortical precursors
555 with *DHCR7* mutations is cholesterol-independent since inhibition of 7-DHC-derived oxysterols
556 via antioxidant treatment can rescue *DHCR7* KD/KO phenotype whereas the cholesterol
557 supplementation cannot.

558 Based on these data, we propose a model where DHCEO binds and activates GR, and in
559 doing so, controls the RTK-mediated neurogenic pathway, TrkB-MEK-C/EBP, and thus fate-
560 decision of developing precursors and neurons. This model is consistent with previous studies
561 showing that an oxysterol structurally similar to DHCEO, OCDO, can bind and regulate GR and
562 its transcriptional activity (Voisin et al., 2017) and ligand-bound GR promoted TrkB
563 phosphorylation, leading to activation of its downstream effectors, MEK and ERK (Jeanneteau et
564 al., 2008). Our model of DHCEO exerting its effect on neurogenesis through GR does not
565 contradict the previous finding by Francis et al., which suggests that Wnt/β-catenin inhibition
566 contributes to precocious neurogenesis (Francis et al., 2016), because activation of GR has been
567 shown to inhibit Wnt/β-catenin signaling in several systems (Olkku and Mahonen, 2009; Zhou et
568 al., 2020).

569 This work represents the first comprehensive characterization of the neurogenic
570 phenotype in SLOS mouse model and SLOS patient-derived NPCs. We demonstrate that the
571 aberrant neural development observed in mice and human NPCs with *DHCR7* mutations occurs
572 in a cholesterol-independent and 7-DHC-derived oxysterol-dependent manner. Successful
573 rescue of the neurogenic phenotype by inhibiting GR or inhibiting the formation of oxysterols
574 with antioxidants pave the wave for potential therapies toward the neurological defects observed
575 in SLOS patients.
576

577 **Acknowledgements**

578 This work was supported by a National Institutes of Health (NIH) grant R01HD092659 (LX) and
579 a grant from Smith-Lemli-Opitz/RSH Foundation. JMH was supported by the University of
580 Washington (UW) Environmental Pathology/ Toxicology Training Program (NIH T32
581 ES007032) and AL was supported by the UW Pharmacological Sciences Training Program (NIH
582 T32 GM007750) and the Institute of Translational Health Sciences TL1 Program (NIH TL1
583 TR002318). We also thank Dr. Carol Ware and Christopher Cavanaugh for technical advices on
584 hiPSC culture.

585 **Author Contributions**

586 HT conceptualized, designed, performed, and analyzed most of the experiments and co-wrote the
587 paper. LX conceptualized, designed experiments, analyzed data and co-wrote the paper. KMH
588 and AL performed and analyzed LC-MS/MS. JMH analyzed RNA-sequencing experiments. DB
589 performed and analyzed docking simulation.

590 **Competing interests**

591 The authors declare no competing interests.

592 **Materials and Methods**

593 ***Animals.*** Animal use was approved by the University of Washington Institutional Animal Care
594 and Use Committee. *Dhcr7* mice (B6.129P2(Cg)-*Dhcr7*^{tm1Gst}/J) were maintained as heterozygous
595 and were genotyped as described previously (Fitzky et al., 2001). The primers used are the
596 following: *Dhcr7*-WT-F: 5'-GGATCTTCTGAGGGCAGCTT-3'; *Dhcr7*-WT-R: 5'-
597 TCTGAACCCTTGGCTGATC-3'; Delta-Mut: 5'-CTAGACCGCGGCTAGAGAAT-3'. For *in*
598 *vitro* transfection, C57BL/6J E12.5 pregnant mice were obtained by time-mating. Mating pairs
599 of wild-type C57BL/6J mice were purchased from Jackson Laboratories (Bar Harbor, ME). All
600 mice had free access to rodent chow and water in a 12-hour dark-light cycle room.

601 ***Plasmids.*** The target sequence for murine *Dhcr7* shRNA was cloned into pLKO-UBI-GFP
602 digested with EcoRI and PacI. pLKO-UBI-GFP was generated by digesting out hPGK promoter
603 from pLKO.3G and ligating ubiquitin promoter (UBI) from pCLX-UBI-VenusN with PacI and
604 BamHI. pLKO.3G was a gift from Christophe Benoist & Diane Mathis (Addgene plasmid #
605 14748; http://n2t.net/addgene:14748; RRID:Addgene_14748) and pCLX-UBI-VenusN was a gift
606 from Patrick Salmon (Addgene plasmid # 27247; http://n2t.net/addgene:27247;
607 RRID:Addgene_27247). cDNAs encoding murine (pCMV-mDHCR7-Myc/DDK) and human
608 DHCR7 (pCMV-hDHCR7-Myc/DDK) were purchased from Origene (MR223420 and
609 RC228922 for murine and human cDNA clone respectively). PB-EF1α-GreenPuro-H1MCS and
610 Super PiggyBac transposase expression vector from System Biosciences (Cat#PBS506A-1 and
611 Cat# PB210PA-1 respectively) were used for clonal analysis.

612 ***Cortical precursor cell cultures.*** Murine cortical precursor cells were cultured as described
613 previously (Barnabe-Heider and Miller, 2003; Tomita et al., 2020). Briefly, mouse cortical
614 precursor cells from cortices were dissected from E12.5 wild-type or *Dhcr7*-KO mouse embryos

615 in ice-cold HBSS (Invitrogen) and transferred into cortical precursor medium. The cortical
616 precursor medium consisted of Neurobasal medium (Invitrogen) with 500 μM L-glutamine
617 (Invitrogen), 2% B27 supplement (Invitrogen), 1% penicillin-streptomycin (Invitrogen) and 40
618 ng/ml FGF2 (BD Biosciences). The dissected tissue was mechanically triturated by a fire-
619 polished glass pipette and plated onto 24-well plates coated with 2% laminin (BD Biosciences)
620 and 1% poly-D-lysine (Sigma Aldrich). Plating density of the cortical precursors was 150,000
621 cells/well in 24-well plates for single embryo cultures and plasmid transfections.
622 ***Human induced pluripotent stem cells (hiPSCs).*** Human fibroblast cell lines (GM03044 and
623 GM05788) isolated from patients with SLOS were obtained from Coriell Institute and
624 reprogrammed as described elsewhere (Okita et al., 2011; Yu et al., 2007). Briefly, $1x10^6$ cells
625 of human fibroblast cells at early passages were trypsinized (0.25% Trypsin/0.5mM EDTA,
626 Gibco) and electroporated with indicated episomal plasmids using Amaxa Basic Nucleofector
627 Kit for primary mammalian fibroblasts, program A-24 (Lonza). 1.0μg pSIN4-EF2-O2S and
628 pSIN4-EF2-N2L were used for each electroporation. The electroporated human fibroblasts were
629 seeded onto a gelatin-coated tissue culture dish and cultured with fibroblast medium (DMEM
630 with 10% FBS, 2mM L-glutamine, 1% non-essential amino acids, 1% sodium pyruvate, and 1%
631 penicillin and streptomycin) for 7 days and re-seeded onto feeder layer cells (irradiated SNL 76/7
632 feeder cells; a gift from Dr. Allan Bradley, Sanger Institute, UK) with hiPSC medium
633 (DMEM/F12 medium with 20% knockout serum replacer, 1% sodium pyruvate, 1% non-
634 essential amino acids, 0.007% 2-mercaptoethanol,1% penicillin and streptomycin, 0.1mM
635 sodium butyrate, 50nM suberoylanilide hydroxamic acid, and 4ng/ml of bFGF) in 100mm tissue
636 culture dishes and continued to be cultured until hiPSC colonies were visible (28 days from
637 electroporation). The hiPSC colonies were then picked and further cultured for expansion.

638 ***Maintenance and Differentiation of hiPSC***. Undifferentiated hiPSCs were cultured and
639 maintained in mTeSR Plus medium (StemCell Technologies) on Matrigel (BD Biosciences)-
640 coated plates prior to the generation of human neural progenitor cells (hNPCs). hNPCs was
641 generated using the STEMdiff SMADi Neural Induction kit (StemCell Technologies) according
642 to the manufacturer's protocol. Briefly, neuralized embryoid bodies (EBs) were generated by
643 culturing small aggregates of hESCs in ultra-low attachment plates (Corning) in STEMdiff
644 SMADi Neural induction medium. EBs were replated and cultured in poly-D-lysine/Laminin-
645 coated plates with the neural induction medium until EBs formed neural rosette formations.
646 Neural rosettes were collected and replated in poly-D-lysine/Laminin-coated plates for hNPCs
647 outgrowth in neural induction medium until hNPCs were ready for the first passage. hNPCs
648 were maintained in STEMdiff Neural Progenitor medium. For neurogenesis of hNPCs, hNPCs
649 were cultured in Neurobasal A medium supplemented with B27 minus vitamin A, 1% penicillin-
650 streptomycin and glutamax (all from Invitrogen) in poly-D-lysine/Laminin-coated plates
651 (Konopka et al., 2012; Usui et al., 2017). For quantification, an average of 700 cells was
652 counted per condition in 5-6 random fields per independent experiment.
653 ***In vitro differentiation of iPSCs.*** For in-vitro differentiation of human iPSCs to the three germ
654 layers, STEMdiff Trilineage Differentiation Kit (StemCell Technologies) was used as described
655 by the manufacturer. Briefly, cells were harvested by Gentle Cell Dissociation Reagent
656 (StemCell Technologies) and plated onto Matrigel-coated 24 well plates with mTeSR1 medium
657 (StemCell Technologies). Cell density and viability were determined using trypan blue
658 exclusion. Cells were seeded at a clonal density of 200,000 cell/cm^2 for ectoderm and endoderm
659 differentiation and 50,000 cell/cm^2 for mesoderm differentiation. 24 hours after plating, cells
660 were switched to the appropriate STEMdiff Trilineage medium for ectoderm, mesoderm and

661 endoderm differentiation. Cells were cultured in the lineage specific medium for 5 days
662 (mesoderm and endoderm lineages) and 7 days (ectoderm lineage) and were harvested and/or
663 fixed for analyses of lineage-specific markers for the three germ layers (Figure 1-Figure
664 Supplement 1).
665 ***Transfection and quantification***. For plasmid transfection of mouse cortical precursors,
666 Lipofectamine LTX and Plus Reagent (Invitrogen) were used as described by the manufacturer.
667 Briefly, 1 μg of DNA and 1 μl of Lipofectamine LTX and Plus Regent in 100 μl of Opti-MEM
668 (both from Invitrogen) were mixed, incubated for 20 min, and added to precursors three hours
669 after plating. For clonal analysis, 1.5 μg DNA, at 1:3 ratio of Super PiggyBac transposase
670 expression vector to shRNA or control plasmids, were incubated as described above and added
671 to cortical precursors three hours after plating. For plasmid transfection of human cortical
672 precursors, Lipofectamine Stem Transfection Reagent (Invitrogen) was used as described by the
673 manufacturer. Briefly, 1μg of DNA and 1μl of Lipofectamine Stem Transfection Reagent were
674 prepared separately in 25μl of Opti-MEM medium (Invitrogen), mixed, incubated for 30 min and
675 added to precursors one day after plating. The target sequences for murine and human *Dhcr7*
676 shRNA were 5'- GGAAGGTGCTTCTTGTTTA-3' and 5'- GGAAGTGGTTTGACTTCAA-3'
677 respectively. The target sequence for the control shRNA was 5'-TCCCAACTGTCACGTTCTC-
678 3'. For quantification, immunostaining and image acquisition were performed, and > 100 cells
679 per condition per experiment were counted and analyzed, and experiments were performed with
680 3 embryos per plasmid transfected and analyzed individually.
681 ***Neurosphere cultures.*** E13.5 cortices from *Dhcr7*$^{+/+}$ or *Dhcr7*$^{-/-}$ embryos were dissected and
682 mechanically dissociated into a single cell suspension by fire-polished glass pipette as previously
683 described (Capecchi and Pozner, 2015; Tomita et al., 2020). Cell density and viability were

684 determined using trypan blue exclusion. Cells were seeded in triplicate at a clonal density of 10
685 cells/μl in 6 well (2 ml/well) ultra-low attachment culture plates (Coster) in serum-free medium
686 supplemented with 20 ng/ml EFG (Sigma), 20 ng/ml FGF2 (Sigma), 2% B27 supplement
687 (Invitrogen) and 2 μg/ml heparin (Sigma). Neurospheres were cultured for 6 days at 37 ºC. To
688 evaluate self-renewal potential, neurospheres were mechanically dissociated into single cell
689 suspensions by fire-polished glass pipette, passed through a 45μm nylon screen cell strainer, and
690 cultured at a clonal density of 2 cells/μl for an additional 6 days.

691 ***Immunocytochemistry and histological analysis.*** For morphometric analysis, immunostaining of
692 tissue sections was performed as described (Capecchi and Pozner, 2015). Briefly, brain sections
693 were permeabilized and blocked in PBST (1X PBS, 0.5% (v/v) Triton X-100) containing 10%
694 NGS for 1 hour. Brain slices were incubated with primary antibodies in PBST with 5% NGS at 4
695 ºC overnight. The sections were incubated with secondary antibodies in PBST with 5% NGS for
696 1-2 hours at room temperature. Sections were counterstained with DAPI (Thermo Fisher
697 Scientific). Slides were mounted in Fluoromount-G anti-fade reagent (Southern Biotech).
698 Digital image acquisition was performed with EVO-FL Imagining System (Thermo Fisher
699 Scientific). For quantification of precursor and neuron numbers, we analyzed sections at the
700 medial-lateral level, counting all marker-positive cells in a 200 μm wide strip of the cortex,
701 extending from the meninges to the ventricle. In all cases, we analyzed at least 3 similar cortical
702 sections/embryo or pup from 3 different embryos or pup per genotype (for a total of at least 9
703 sections per genotype).

704 ***Antibodies***. The primary antibodies used for immunostaining were chicken anti-GFP (1:1000;
705 Abcam), rabbit anti-Dhcr7 (1:100; Thermo Fisher Scientific), rabbit anti-Sox2 (1:200; Cell
706 Signaling Technology), rabbit anti-Pax6 (1:1000; Covance), mouse anti-Ki67 (1:200; BD

707 Biosciences), mouse anti-βIII-tubulin (1:1000; Covance), rabbit anti-βIII-tubulin (1:1000;
708 Covance), rabbit anti-Tbr1 (1:500; Abcam), mouse anti-Satb2 (1:400; Abcam), rat anti-Ctip2
709 (1:500; Abcam), and rabbit anti-cleaved caspase 3 (1:400; Cell Signaling Technology), mouse
710 anti-Nestin (1:1000; StemCell Technologies), rabbit anti-Brachyury (1:200; R&D Systems), goat
711 anti-NCAM (1:200; R&D Systems), goat anti-Sox17 (1:200; R&D Systems), rabbit anti-Foxa2
712 (1:1000; Abcam). The secondary antibodies used for immunostaining were Rhodamine
713 (TRITC)-conjugated goat anti-mouse and anti-rabbit IgG (1:500; Jackson ImmunoResearch
714 Laboratories) and Alexa Fluor 488-conjugated goat anti-mouse, anti-rat and anti-rabbit IgG
715 (1:800; Jackson ImmunoResearch Laboratories), Alexa Flour 488-conjugated donkey anti-goat
716 IgG (1:800; Jackson ImmunoResearch Laboratories), Rhodamine (TRITC)-conjugated donkey
717 anti-goat (1:200; Jaclson ImmunoResearch Laboratories). The primary antibodies used for
718 immunoblotting were rabbit anti-Dhcr7 (1:1000; Abcam), rabbit anti-GAPDH (1:5000; Santa
719 Cruz Biotechnology), rabbit anti Erk1/2 (1:5000; Santa Cruz Biotechnology), rabbit anti-TrkB
720 (1:1000; Cell Signaling Technology), rabbit anti-phospho-TrkB (1:1000; Cell Signaling
721 Technology), rabbit anti-glucocorticoid receptor (1:1000; Cell Signaling Technology), rabbit
722 anti-phospho-glucocorticoid receptor (1:1000; Cell Signaling Technology), rabbit anti-MEK
723 (1:1000; Cell Signaling Technology), rabbit anti-phospho-MEK (1:1000; Cell Signaling), rabbit
724 anti-phospho-cebpβ (1:1000; Cell signaling Technology) and rabbit anti-cebpβ (1:1000; Cell
725 Signaling Technology), rabbit anti-Pax6 (1:1000; Covance), mouse anti-Nestin (1:1000;
726 StemCell Technologies), rabbit anti-Brachyury (1:200; R&D Systems), rabbit anti-Tbr2 (1:500;
727 Abcam), goat anti-Sox17 (1:200; R&D Systems), rabbit anti-Foxa2 (1:1000; Abcam). The
728 secondary antibodies used for immunoblotting were HRP-conjugated goat anti-mouse IgG
729 (1:5000; Jackson ImmunoResearch Laboratories) and anti-rabbit IgG (1:10,000; Jackson

730 ImmunoResearch Laboratories), HRP-conjugated donkey anti-goat IgG (1:1000; Jackson
731 ImmunoResearch Laboratories).
732 ***RT-PCR.*** Total RNA was isolated with Trizol and cDNA was prepared using the SuperScript III
733 Reverse Transcriptase kit (Invitrogen) according to the manufacture's protocols. Primer
734 sequences are the following: *Dhcr7*-F: 5'-TATGAGGTGAATGGGCTGCA-3'; *Dhcr7*-R: 5'-
735 GGTTAATGAGGGTCCAGGCT -3'; *β-actin*-F: 5'-GATGACGATATCGCTGCGCTG-3'; *β-*
736 *actin*-R: 5'- GTACGACCAGAGGCATACAGG-3'. All PCR products were single bands with
737 predicted molecular weights and confirmed by DNA sequencing.
738 ***Quantitative PCR***. Total RNA was extracted with Tri-Reagent (Sigma) treated with DNAse I
739 (Fermentas, Thermo Scientific, Waltham, MA, USA) and cDNA was synthesized from 1μg of
740 RNA using the SuperScript IV Reverse Transcriptase Kit (Invitrogen) according to the
741 manufacturer's protocols. Quantitative PCR was performed using Taqman Fast Advance Mater
742 Mix (Thermo Fisher Scientific) and Taqman probes targeted against either *Dhcr7*
743 (Mm01164321_m1) or *β-Actin* (Mm00607939_s1). *β-Actin* mRNA was used as an endogenous
744 control for all reactions, and all reactions were performed in triplicate. Quantitative PCR was
745 performed and analyzed using StepOne Plus Real-Time PCR system (ThermoFisher Scientific).
746 ***Western Blotting.*** Embryonic cortices or neurosphere cultures were lysed in RIPA buffer (50
747 mM Tri pH8, 150mM NaCl, 1% NP-40, 0.1% SDS, 1mM EDTA) containing 1mM PMSF
748 (phenylmethanesulfonyl fluoride), 1mM sodium vanadate, 20mM sodium fluoride 10 μg/ml
749 aprotinin and 10 μg/ml leupeptin. 10-20 μg of protein lysate was electrophoresed, and western
750 blots were performed as described previously (Barnabe-Heider and Miller, 2003).
751 ***RNA sequencing and data analysis***. Raw RNA sequencing reads in FASTQ format were
752 mapped to the human genome using HISAT (https://ccb.jhu.edu/software/hisat/; Last accessed

753 January 22, 2021), and format conversions were performed using Samtools. Cufflinks
754 (http://cole-trapnell-lab.github.io/cufflinks/; Last accessed January 22, 2021) was used to
755 estimate relative abundances of transcripts from each RNA sample. Cuffdiff, a module of
756 Cufflinks, was then used to determine differentially expressed genes (DEGs) between WT and
757 KO hNPCs. DEGs met the following criteria: adjusted p value < .05 (corresponding to the
758 allowed false discovery rate of 5%) and fold-change > 1.5 between genotypes. A two-way
759 hierarchical clustering dendrogram (complete-linkage method, Euclidean distance scale) of
760 DEGs was used to visualize biological variability among samples, generated by R software using
761 the "pheatmap" package (https://cran.r-project.org/web/packages/pheatmap/). To elucidate
762 biological functions of DEGs, the Core Analysis feature of Ingenuity Pathway Analysis (IPA®,
763 Qiagen) was used to identify significantly enriched Diseases and Biological Functions related to
764 the nervous system. Network interactions among DEGs involved in the Biological Function
765 "development of the central nervous system" were assessed using STRING (Search Tool for the
766 Retrieval of Interacting Genes/Proteins) analysis, set at the highest confidence interaction score
767 and only connected nodes displayed (https://string-db.org/cgi/input.pl?sessionId=xCahIfrzvltC;
768 Last accessed January 22, 2021). Enriched KEGG (Kyoto Encyclopedia of Genes and Genomes)
769 pathways were identified among DEGs in the STRING network. Finally, a Venn diagram was
770 generated to demonstrate the overlap between genes dysregulated in KO hNPCs and genes in the
771 SFARI database, a collection of genes implicated in autism susceptibility (https://gene.sfari.org/;
772 Last accessed January 22, 2021). Raw data of the RNA sequencing has been deposited at Dryad
773 (https://doi.org/10.5061/dryad.zw3r2287f; available upon publication). The list of differentially
774 expressed genes can be found in Supplementary File 2 (Excel).

775 ***Oxysterol and Sterol Analysis.*** Cell pellets were resuspended in 300 μL of 1X PBS and lysed by
776 sonication in an ice bath for 30 min. Protein determination was performed using the BioRad DC
777 protein mass assay (BioRad, Hercules, CA). Internal standard mixtures for sterols and oxysterols
778 analysis were added to each sample (see Tables S1-4 for a list of standards and their
779 concentrations used). Lipid extraction was performed using the Folch method as described
780 previously (Fliesler et al., 2018; Folch et al., 1957; Herron et al., 2018). The dried lipid extract
781 was reconstituted with 200 μL of methylene chloride and stored at -80 ºC until analysis. Prior to
782 analysis, 50 μL of extract was transferred to into glass LC vials, dried under argon, and
783 reconstituted with 50 μL of 90% methanol in water with 0.1% formic acid. For tissue samples,
784 sterol and oxysterol internal standard mixtures were added to whole tissues, which were
785 subsequently homogenized in 4 mL Folch solution with 1 mL 0.9% NaCl. The dried lipid extract
786 was reconstituted with 0.5 mL (for tissues <50 mg), 1.0 mL (tissues >50 <100 mg) or 1.5 mL
787 (>100 mg) of methylene chloride. Prior to analysis, 50 μL of lipid extract (30 μL for tissues
788 >100 mg) was transferred into glass LC vials, dried under argon, and reconstituted with 50 μL
789 90% methanol in water with 0.1% formic acid. Determination of oxysterol and sterol
790 concentrations in cells and tissues was performed by ultra-performance liquid chromatography
791 (UPLC) tandem mass spectrometry (MS/MS) on a SCIEX 6500 triple quadrupole mass
792 spectrometer (for oxysterols) or a SCIEX 4000 QTRAP (for sterols) mass spectrometer with
793 atmospheric pressure chemical ionization (APCI) coupled to a Waters Acquity UPLC system, as
794 described previously (Fliesler et al., 2018; Herron et al., 2018). Briefly, sterols and oxysterols
795 were separated by reversed phase chromatography on a C18 column (1.7 mm, 2.1 x 100 mm,
796 Phenomenex Kinetex) using a 15 min isocratic gradient of 90% methanol with 0.1% formic acid
797 at a flow of 0.4 mL/min. Selective reaction monitoring (SRM) was used to monitor the

798 dehydration of the sterol and oxysterol $[M+H]^+$ ions to generate $[M+H-H_2O]^+$ ions (See Table
799 S1-4 for a list of retention times and MS/MS transitions for the standards used). The APCI
800 parameters were as follows: nebulizer current, 3 mA; temperature, 350 ºC; curtain gas, 20 psi;
801 ion source gas, 55 psi. The MS conditions for SRM analysis were as follows: declustering
802 potential, 80 V; entrance potential, 10 V; collision energy, 25 V; collision cell exit potential, 20
803 V. Data analysis was performed with Analyst (v. 1.6.2) Quantitation Wizard. Analyte
804 concentrations in cells and tissues were determined relative to the internal standard levels and the
805 relative response factor (RRF) of each analyte calculated from a mixture of sterol and oxysterol
806 standards and internal standards. Concentrations were normalized to cell protein weight or tissue
807 weight.
808 ***Docking simulation.*** Docking simulation was performed with Autodock Vina 1.1.2. The model
809 ligands and 3D models were built and generated by Openbabel 2.3.2. Crystal structure of
810 glucococorticoid receptor and docking of cortisol to glucocorticoid receptor were from crystal
811 structure 4p6w available from Protein Data Bank (http://www.rcsb.org/structure/4p6w).
812 ***Statistical analysis.*** In general, three biological replicates were used for each experiment based
813 on the strong phenotype observed in the *Dhcr7*-KO SLOS model and our previous publication
814 showing the large differences in oxysterols and sterol levels in WT and KO brains at birth (Xu et
815 al., 2011). For culturing of mouse cortical precursors or neurospheres from single embryos, one
816 litter is considered a biological replicate. For hNPC culture, each separate preparation of hNPC
817 from hiPSC is considered a biological replicate. For *in vivo* study, one litter is considered a
818 biological replicate. Statistical analyses were performed using two-tailed Student's *t*-test
819 assuming unequal variance when comparing two different groups unless otherwise indicated in
820 the text. For immunostaining of cell culture or tissue sections, at least three technical replicates

821 per biological replicate were performed. To analyze the multi-group neuroanatomical studies, we
822 used one-way ANOVA unless otherwise indicated in the text. Significant interactions or main
823 effects were further analyzed using Newman-Keuls post-hoc tests. All statistical tests were
824 performed using Microsoft Excel or Prism 8 (GraphPad). In all cases, error bars indicate standard
825 error of the mean.
826
827
828
829
830
831
832
833
834
835
836
837
838
839
840
841
842
843

844 **Figure Supplements**

845 **Figure 1-Figure Supplement 1. Characterization of the pluripotency of SLOS-derived**
846 **human iPSCs.** Related to Figure 1. Pluripotency of SLOS patient derived human iPSC lines,
847 3044 and 5788 were characterized. (A) Representative images of established SLOS patient
848 derived human iPSC lines (3044 and 5788) and human iPSC line from healthy individual
849 (emhf2). (B) RT-PCR analysis of hES cell marker genes in human iPSCs derived from SLOS
850 patients (3044 and 5788) and healthy individual (emhf2). Primers used for Oct3/4, Sox2, Klf4
851 and c-Myc specifically amplified endogenous transcripts but not transgenic transcripts. (C)
852 Immunostaining confirming in-vitro differentiation of SLOS patient derived human iPSCs (3044
853 and 5788) into all three germ layers. (D) RT-PCR analyses and Western blot analyses of
854 differentiation markers for the three germ layers.
855
856
857 **Figure 1-Figure Supplement 2. Loss of *DHCR7* alleles causes decreased proliferation and**
858 **increased neurogenesis in human cortical precursors.** (A) Images of cultured human cortical
859 precursors immunostained for Dhcr7 (red) and Sox2 or Nestin (green). (B-D) Human SLOS-
860 patient-derived (SLOS 3044 and SLOS 5788) and unaffected-patient-derived cortical precursors
861 were cultured for 3 days and analyzed. (B) Cells were immunostained for Ki67 (green) and βIII-
862 tubulin (red) after 3 days and quantified the proportions of Ki67+ (C) and βIII-tubulin+ cells (D).
863 Scale Bar = 50 μm. *, $p < 0.001$; n = 3 biological replicates per genotype.
864
865 **Figure 2-Figure Supplement 1. Cholesterol precursor 7-DHC and 7-DHC-derived**
866 **Oxysterols are accumulated *in* SLOS-derived human iPSCs and NPCs.** Related to Figure 2.
867 SLOS patient derived hiPSCs and NPCs (3044 and 5788) along hiPSCs and NPC from healthy
868 individual (emhf2) were cultured and used for LC-MS/MS analysis sterols and oxysterols.
869 Quantitation of cholesterol, its precursors and accumulated 7-DHC derived oxysterols in SLOS
870 patient derived hiPSCs and hiPSCs from healthy individuals (A) and in SLOS patient derived
871 NPCs and NPCs from healthy individuals (B).
872
873 **Figure 3-Figure Supplement 1. Rescue of the neurogenesis phenotype in *Dhcr7*-knockdown**
874 **mouse cortical precursors by human *DHCR7* cDNA expression vector.** Related to Figure 3.
875 Potential off-target effects of murine *Dhcr7* shRNAs were determined. Human *DHCR7* cDNA
876 expressing vectors transfected murine NPCs with either murine Dhcr7 shRNA vector or control
877 shRNA vectors. The transfected cells were cultured for 3 days, immunostained and analyzed for
878 proliferation marker, Ki67 or neuronal marker, βIII tubulin. (A) Cultures were immunostained
879 for EGFP-mDhcr7shRNA and proliferation marker Ki67, the proportion of total EGFP+ cells
880 that were also positive for Ki67 was quantified. (B) Cultures were immunostained for EGFP-
881 mDhcr7shRNA and neuronal marker, βIII tubulin, the proportion of total EGFP+ cells that were
882 also positive for βIII tubulin was quantified.
883

884 **Figure 7-Figure Supplement 1. Antioxidants rescue the neurogenic phenotype in human**
885 **and murine NPCs with *Dhcr7* mutations.** Related to Figure 7. (A) Structures of DHCEO and
886 known ligands of GR, OCDO and cortisol. (B, D) Another SLOS hNPC line (SLOS 5788) and
887 mNPCs from E12.5 *Dhcr7*$^{-/-}$ and *Dhcr7*$^{+/+}$ embryonic cortices were cultured and treated with

888 cholesterol, vitamin E, vitamin C, vitamin E/C or glutathione (GSH). The cells were
889 immunostained for βIII-tubulin and DAPI three days after plated. (C) Quantification of the
890 proportion of βIII-tubulin positive cells in wild type hNPCs and SLOS hNPCs treated with
891 cholesterol or antioxidants. (D) Quantification of the proportion of βIII-tubulin positive cells in
892 *Dhcr7*$^{-/-}$ and *Dhcr7*$^{+/+}$ NPCs treated with cholesterol or antioxidants. Error bars indicate SEM. *,
893 $p < 0.001$. n = 3 per experiment. Scale Bar = 50 μm.
894
895
896
897
898
899
900
901
902
903
904
905
906
907
908
909
910
911
912
913

914 **Supplementary File 1**
915
916 **Table S1. Retention times and MS/MS transitions for oxysterol internal standards. Relate to**
917 **Figure 2 and S3.**
918
919 **Table S2. Retention times and MS/MS transitions for all oxysterol standards. Relate to**
920 **Figure 2 and S3.**
921
922 **Table S3. Retention times and MS/MS transitions for sterol internal standards. Relate to**
923 **Figure 2 and S3.**
924
925 **Table S4. Retention times and MS/MS transitions for sterol standards. Relate to Figure 2**
926 **and S3.**
927
928 **Table S5. Ingenuity Pathway Analysis (IPA®) reveals "development of the central nervous**
929 **system" as one of the top 10 enriched Diseases and Biological Functions related to the**
930 **nervous system.** Related to Figure S1. DEGs were further analyzed with (IPA®) to identify the
931 most enriched biological functions related to the nervous system in SLOS mutant NPCs. The
932 table below shows the top ten enriched terms corresponding to Diseases/Bio-functions along
933 with the *p*-value and overlapping number of genes in the dataset.
934
935 **Figure S1. Perturbation in *DHCR7* causes gene expression changes in neurogenic**
936 **pathways in human NPCs.** (A) Hierarchical clustering heatmap of differentially expressed
937 genes show distinct expression pattern changes in transcript abundance for SLOS mutant NPCs
938 as compared to wild type. Red color represents increase in abundance, blue color represents
939 relative decrease, and white color represents no change. (B) Enriched KEGG pathways identified
940 among DEGs from SLOS mutant NPCs and involved in the Biological Function "development
941 of the central nervous system", identified by Ingenuity Pathway Analysis (see Supporting
942 Information). Color of bar corresponds to DEGs in the STRING network that are in enriched
943 pathways. (C) String analysis of DEGs from SLOS mutant NPCs and involved in the Biological
944 Function "Development of the central nervous system" identified by Ingenuity Pathway
945 Analysis. Parameters of high confidence have been applied and only connected nodes are
946 displayed. Arrows indicate whether the gene was up- or down-regulated. Color of DEG
947 corresponds to enriched KEGG pathway. n =3 biological replicates per genotype; DEGs met the
948 criteria of fold-change > 1.5 between genotypes and adjusted p-value < 0.05.
949
950

951 **Supplementary File 2**
952
953 **Table S6 (Excel file). List of differentially expressed genes in SLOS hNPCs relative to wild-**
954 **type hNPCs. Relate to Figure S1.**
955

956

957 **References**
958

959 Barnabe-Heider, F., and Miller, F.D. (2003). Endogenously produced neurotrophins regulate
960 survival and differentiation of cortical progenitors via distinct signaling pathways. J Neurosci *23*,
961 5149-5160.

962 Bartkowska, K., Paquin, A., Gauthier, A.S., Kaplan, D.R., and Miller, F.D. (2007). Trk signaling
963 regulates neural precursor cell proliferation and differentiation during cortical development.
964 Development *134*, 4369-4380. doi: 10.1242/dev.008227.

965 Bonni, A., Brunet, A., West, A.E., Datta, S.R., Takasu, M.A., and Greenberg, M.E. (1999). Cell
966 survival promoted by the Ras-MAPK signaling pathway by transcription-dependent and -
967 independent mechanisms. Science *286*, 1358-1362. doi: 10.1126/science.286.5443.1358.

968 Bukelis, I., Porter, F.D., Zimmerman, A.W., and Tierney, E. (2007). Smith-Lemli-Opitz
969 syndrome and autism spectrum disorder. Am J Psychiatry *164*, 1655-1661. doi: 164/11/1655
970 [pii] 10.1176/appi.ajp.2007.07020315.

971 Byrne, E.F., Sircar, R., Miller, P.S., Hedger, G., Luchetti, G., Nachtergaele, S., Tully, M.D.,
972 Mydock-McGrane, L., Covey, D.F., Rambo, R.P.*, et al.* (2016). Structural basis of Smoothened
973 regulation by its extracellular domains. Nature *535*, 517-522. doi: 10.1038/nature18934.

974 Capecchi, M.R., and Pozner, A. (2015). ASPM regulates symmetric stem cell division by tuning
975 Cyclin E ubiquitination. Nat Commun *6*, 8763. doi: 10.1038/ncomms9763.

976 Chenn, A., and Walsh, C.A. (2002). Regulation of cerebral cortical size by control of cell cycle
977 exit in neural precursors. Science *297*, 365-369. doi: 10.1126/science.1074192.

978 Corcoran, R.B., and Scott, M.P. (2006). Oxysterols stimulate Sonic hedgehog signal transduction
979 and proliferation of medulloblastoma cells. Proc Natl Acad Sci U S A *103*, 8408-8413. doi:
980 10.1073/pnas.0602852103.

981 Dietschy, J.M., and Turley, S.D. (2004). Cholesterol metabolism in the central nervous system
982 during early development and in the mature animal. J Lipid Res *45*, 1375-1397. doi:
983 10.1194/jlr.R400004-JLR200 R400004-JLR200 [pii].

984 DiSalvo, C.V., Zhang, D., and Jacobberger, J.W. (1995). Regulation of NIH-3T3 cell G1 phase
985 transit by serum during exponential growth. Cell Prolif *28*, 511-524. doi: 10.1111/j.1365-
986 2184.1995.tb00089.x.

987 Doba, T., Burton, G.W., and Ingold, K.U. (1985). Antioxidant and co-antioxidant activity of
988 vitamin C. The effect of vitamin C, either alone or in the presence of vitamin E or a water-
989 soluble vitamin E analogue, upon the peroxidation of aqueous multilamellar phospholipid

990 liposomes. Biochimica et Biophysica Acta (BBA) - Lipids and Lipid Metabolism *835*, 298-303.
991 doi: https://doi.org/10.1016/0005-2760(85)90285-1.

992 DuSell, C.D., Umetani, M., Shaul, P.W., Mangelsdorf, D.J., and McDonnell, D.P. (2008). 27-
993 Hydroxycholesterol Is an Endogenous Selective Estrogen Receptor Modulator. Molecular
994 Endocrinology *22*, 65-77. doi: 10.1210/me.2007-0383.

995 Ferreira, L.G., Dos Santos, R.N., Oliva, G., and Andricopulo, A.D. (2015). Molecular docking
996 and structure-based drug design strategies. Molecules *20*, 13384-13421. doi:
997 10.3390/molecules200713384.

998 Fitzky, B.U., Moebius, F.F., Asaoka, H., Waage-Baudet, H., Xu, L., Xu, G., Maeda, N.,
999 Kluckman, K., Hiller, S., Yu, H.*, et al.* (2001). 7-Dehydrocholesterol-dependent proteolysis of
1000 HMG-CoA reductase suppresses sterol biosynthesis in a mouse model of Smith-Lemli-
1001 Opitz/RSH syndrome. J Clin Invest *108*, 905-915. doi: 10.1172/jci12103.

1002 Fitzky, B.U., Witsch-Baumgartner, M., Erdel, M., Lee, J.N., Paik, Y.K., Glossmann, H.,
1003 Utermann, G., and Moebius, F.F. (1998). Mutations in the Delta 7-sterol reductase gene in
1004 patients with the Smith-Lemli-Opitz syndrome. Proc Natl Acad Sci U S A *95*, 8181-8186.

1005 Fliesler, S.J., Peachey, N.S., Herron, J., Hines, K.M., Weinstock, N.I., Ramachandra Rao, S., and
1006 Xu, L. (2018). Prevention of Retinal Degeneration in a Rat Model of Smith-Lemli-Opitz
1007 Syndrome. Sci Rep *8*, 1286. doi: 10.1038/s41598-018-19592-8.

1008 Folch, J., Lees, M., and Sloane Stanley, G.H. (1957). A simple method for the isolation and
1009 purification of total lipides from animal tissues. J Biol Chem *226*, 497-509.

1010 Francis, K.R., Ton, A.N., Xin, Y., O'Halloran, P.E., Wassif, C.A., Malik, N., Williams, I.M.,
1011 Cluzeau, C.V., Trivedi, N.S., Pavan, W.J.*, et al.* (2016). Modeling Smith-Lemli-Opitz syndrome
1012 with induced pluripotent stem cells reveals a causal role for Wnt/beta-catenin defects in neuronal
1013 cholesterol synthesis phenotypes. Nat Med *22*, 388-396. doi: 10.1038/nm.4067.

1014 Herron, J., Hines, K.M., and Xu, L. (2018). Assessment of Altered Cholesterol Homeostasis by
1015 Xenobiotics Using Ultra-High Performance Liquid Chromatography-Tandem Mass
1016 Spectrometry. Curr Protoc Toxicol *78*, e65. doi: 10.1002/cptx.65.

1017 Huang, P., Zheng, S., Wierbowski, B.M., Kim, Y., Nedelcu, D., Aravena, L., Liu, J., Kruse,
1018 A.C., and Salic, A. (2018). Structural Basis of Smoothened Activation in Hedgehog Signaling.
1019 Cell *174*, 312-324. doi: 10.1016/j.cell.2018.04.029.

1020 Jeanneteau, F., Garabedian, M.J., and Chao, M.V. (2008). Activation of Trk neurotrophin
1021 receptors by glucocorticoids provides a neuroprotective effect. Proc Natl Acad Sci U S A *105*,
1022 4862-4867. doi: 10.1073/pnas.0709102105.

1023 Jiang, X.S., Wassif, C.A., Backlund, P.S., Song, L., Holtzclaw, L.A., Li, Z., Yergey, A.L., and
1024 Porter, F.D. (2010). Activation of Rho GTPases in Smith-Lemli-Opitz syndrome:
1025 pathophysiological and clinical implications. Hum Mol Genet *19*, 1347-1357. doi:
1026 10.1093/hmg/ddq011.

1027 Konopka, G., Wexler, E., Rosen, E., Mukamel, Z., Osborn, G.E., Chen, L., Lu, D., Gao, F., Gao,
1028 K., Lowe, J.K.*, et al.* (2012). Modeling the functional genomics of autism using human neurons.
1029 Molecular Psychiatry *17*, 202-214. doi: 10.1038/mp.2011.60.

1030 Korade, Z., Xu, L., Harrison, F.E., Ahsen, R., Hart, S.E., Folkes, O.M., Mirnics, K., and Porter,
1031 N.A. (2014). Antioxidant Supplementation Ameliorates Molecular Deficits in Smith-Lemli-
1032 Opitz Syndrome. Biol Psychiatry *75*, 215-222. doi: S0006-3223(13)00591-X [pii]
1033 10.1016/j.biopsych.2013.06.013.

1034 Korade, Z., Xu, L., Shelton, R., and Porter, N.A. (2010). Biological activities of 7-
1035 dehydrocholesterol-derived oxysterols: implications for Smith-Lemli-Opitz syndrome. J Lipid
1036 Res *51*, 3259-3269. doi: jlr.M009365 [pii] 10.1194/jlr.M009365.

1037 Menard, C., Hein, P., Paquin, A., Savelson, A., Yang, X.M., Lederfein, D., Barnabe-Heider, F.,
1038 Mir, A.A., Sterneck, E., Peterson, A.C.*, et al.* (2002). An essential role for a MEK-C/EBP
1039 pathway during growth factor-regulated cortical neurogenesis. Neuron *36*, 597-610. doi:
1040 10.1016/s0896-6273(02)01026-7.

1041 Molyneaux, B.J., Arlotta, P., Menezes, J.R., and Macklis, J.D. (2007). Neuronal subtype
1042 specification in the cerebral cortex. Nat Rev Neurosci *8*, 427-437. doi: 10.1038/nrn2151.

1043 Myers, B.R., Neahring, L., Zhang, Y., Roberts, K.J., and Beachy, P.A. (2017). Rapid, direct
1044 activity assays for Smoothened reveal Hedgehog pathway regulation by membrane cholesterol
1045 and extracellular sodium. Proc Natl Acad Sci U S A *114*, E11141-E11150. doi:
1046 10.1073/pnas.1717891115.

1047 Okita, K., Matsumura, Y., Sato, Y., Okada, A., Morizane, A., Okamoto, S., Hong, H.,
1048 Nakagawa, M., Tanabe, K., Tezuka, K.*, et al.* (2011). A more efficient method to generate
1049 integration-free human iPS cells. Nat Methods *8*, 409-412. doi: 10.1038/nmeth.1591.

1050 Olkku, A., and Mahonen, A. (2009). Calreticulin mediated glucocorticoid receptor export is
1051 involved in β-catenin translocation and Wnt signalling inhibition in human osteoblastic cells.
1052 Bone *44*, 555-565. doi: https://doi.org/10.1016/j.bone.2008.11.013.

1053 Porter, F.D., and Herman, G.E. (2011). Malformation syndromes caused by disorders of
1054 cholesterol synthesis. J Lipid Res *52*, 6-34. doi: jlr.R009548 [pii] 10.1194/jlr.R009548.

1055 Porter, J.A., Young, K.E., and Beachy, P.A. (1996). Cholesterol modification of hedgehog
1056 signaling proteins in animal development. Science *274*, 255-259.

1057 Porter, N.A., Xu, L., and Pratt, D.A. (2020). Reactive Sterol Electrophiles: Mechanisms of
1058 Formation and Reactions with Proteins and Amino Acid Nucleophiles. Chemistry *2*, 390-417.
1059 doi: 10.3390/chemistry2020025.

1060 Raleigh, D.R., Sever, N., Choksi, P.K., Sigg, M.A., Hines, K.M., Thompson, B.M., Elnatan, D.,
1061 Jaishankar, P., Bisignano, P., Garcia-Gonzalo, F.R.*, et al.* (2018). Cilia-Associated Oxysterols
1062 Activate Smoothened. Mol Cell *72*, 316-327 e315. doi: 10.1016/j.molcel.2018.08.034.

1063 Sever, N., Mann, R.K., Xu, L., Snell, W.J., Hernandez-Lara, C.I., Porter, N.A., and Beachy, P.A.
1064 (2016). Endogenous B-ring oxysterols inhibit the Hedgehog component Smoothened in a manner
1065 distinct from cyclopamine or side-chain oxysterols. Proc Natl Acad Sci U S A *113*, 5904-5909.
1066 doi: 10.1073/pnas.1604984113.

1067 Sheng, R., Kim, H., Lee, H., Xin, Y., Chen, Y., Tian, W., Cui, Y., Choi, J.C., Doh, J., Han, J.K.*,*
1068 *et al.* (2014). Cholesterol selectively activates canonical Wnt signalling over non-canonical Wnt
1069 signalling. Nat Commun *5*, 4393. doi: 10.1038/ncomms5393.

1070 Sikora, D., Pettit-Kekel, K., Penfield, J., Merkens, L., and Steiner, R. (2006). The near universal
1071 presence of autism spectrum disorders in children with Smith-Lemli-Opitz syndrome. Am J Med
1072 Genet *140A*, 1511-1518. doi: 10.1002/(issn)1552-4833.

1073 Theofilopoulos, S., Wang, Y., Kitambi, S.S., Sacchetti, P., Sousa, K.M., Bodin, K., Kirk, J.,
1074 Salto, C., Gustafsson, M., Toledo, E.M.*, et al.* (2013). Brain endogenous liver X receptor ligands
1075 selectively promote midbrain neurogenesis. Nat Chem Biol *9*, 126-133. doi:
1076 10.1038/nchembio.1156.

1077 Thurm, A., Tierney, E., Farmer, C., Albert, P., Joseph, L., Swedo, S., Bianconi, S., Bukelis, I.,
1078 Wheeler, C., Sarphare, G.*, et al.* (2016). Development, behavior, and biomarker characterization
1079 of Smith-Lemli-Opitz syndrome: an update. J Neurodev Disord *8*, 12. doi: 10.1186/s11689-016-
1080 9145-x.

1081 Tierney, E., Bukelis, I., Thompson, R.E., Ahmed, K., Aneja, A., Kratz, L., and Kelley, R.I.
1082 (2006). Abnormalities of cholesterol metabolism in autism spectrum disorders. Am J Med Genet
1083 B *141B*, 666-668. doi: 10.1002/ajmg.b.30368.

1084 Tint, G.S., Irons, M., Elias, E.R., Batta, A.K., Frieden, R., Chen, T.S., and Salen, G. (1994).
1085 Defective cholesterol biosynthesis associated with the Smith-Lemli-Opitz syndrome. N Engl J
1086 Med *330*, 107-113.

1087 Tint, G.S., Seller, M., Hughes-Benzie, R., Batta, A.K., Shefer, S., Genest, D., Irons, M., Elias,
1088 E., and Salen, G. (1995). Markedly increased tissue concentrations of 7-dehydrocholesterol
1089 combined with low levels of cholesterol are characteristic of the Smith-Lemli-Opitz syndrome. J
1090 Lipid Res *36*, 89-95.

1091 Tomita, H., Cornejo, F., Aranda-Pino, B., Woodard, C.L., Rioseco, C.C., Neel, B.G., Alvarez,
1092 A.R., Kaplan, D.R., Miller, F.D., and Cancino, G.I. (2020). The Protein Tyrosine Phosphatase
1093 Receptor Delta Regulates Developmental Neurogenesis. Cell Rep *30*, 215-228 e215. doi:
1094 10.1016/j.celrep.2019.11.033.

1095 Usui, N., Araujo, D.J., Kulkarni, A., Co, M., Ellegood, J., Harper, M., Toriumi, K., Lerch, J.P.,
1096 and Konopka, G. (2017). Foxp1 regulation of neonatal vocalizations via cortical development.
1097 Genes Dev *31*, 2039-2055. doi: 10.1101/gad.305037.117.

1098 Voisin, M., de Medina, P., Mallinger, A., Dalenc, F., Huc-Claustre, E., Leignadier, J., Serhan,
1099 N., Soules, R., Ségala, G., Mougel, A.*, et al.* (2017). Identification of a tumor-promoter
1100 cholesterol metabolite in human breast cancers acting through the glucocorticoid receptor.
1101 Proceedings of the National Academy of Sciences *114*, E9346. doi: 10.1073/pnas.1707965114.

1102 Wassif, C.A., Maslen, C., Kachilele-Linjewile, S., Lin, D., Linck, L.M., Connor, W.E., Steiner,
1103 R.D., and Porter, F.D. (1998). Mutations in the human sterol Delta(7)-reductase gene at 11q12-
1104 13 cause Smith-Lemli-Opitz syndrome. American Journal of Human Genetics *63*, 55-62.

1105 Xu, L., Davis, T.A., and Porter, N.A. (2009). Rate Constants for Peroxidation of Polyunsaturated
1106 Fatty Acids and Sterols in Solution and in Liposomes. J Am Chem Soc *131*, 13037-13044.

1107 Xu, L., Korade, Z., and Porter, N.A. (2010). Oxysterols from free radical chain oxidation of 7-
1108 dehydrocholesterol: product and mechanistic studies. J Am Chem Soc *132*, 2222-2232. doi:
1109 10.1021/ja9080265.

1110 Xu, L., Korade, Z., Rosado, D.A., Jr., Mirnics, K., and Porter, N.A. (2013). Metabolism of
1111 oxysterols derived from nonenzymatic oxidation of 7-dehydrocholesterol in cells. J Lipid Res *54*,
1112 1135-1143. doi: 10.1194/jlr.M035733
1113 jlr.M035733 [pii].

1114 Xu, L., Korade, Z., Rosado, D.A., Liu, W., Lamberson, C.R., and Porter, N.A. (2011). An
1115 oxysterol biomarker for 7-dehydrocholesterol oxidation in cell/mouse models for Smith-Lemli-
1116 Opitz syndrome. J Lipid Res *52*, 1222-1233. doi: jlr.M014498 [pii] 10.1194/jlr.M014498.

1117 Xu, L., Mirnics, K., Bowman, A.B., Liu, W., Da, J., Porter, N.A., and Korade, Z. (2012).
1118 DHCEO accumulation is a critical mediator of pathophysiology in a Smith-Lemli-Opitz
1119 syndrome model. Neurobiol Dis *45*, 923-929. doi: S0969-9961(11)00386-X [pii]
1120 10.1016/j.nbd.2011.12.011.

1121 Yang, S.H., Sharrocks, A.D., and Whitmarsh, A.J. (2013). MAP kinase signalling cascades and
1122 transcriptional regulation. Gene *513*, 1-13. doi: 10.1016/j.gene.2012.10.033.

1123 Yin, H., Xu, L., and Porter, N.A. (2011). Free radical lipid peroxidation: mechanisms and
1124 analysis. Chem Rev *111*, 5944-5972. doi: 10.1021/cr200084z.

1125 Yu, J., Vodyanik, M.A., Smuga-Otto, K., Antosiewicz-Bourget, J., Frane, J.L., Tian, S., Nie, J.,
1126 Jonsdottir, G.A., Ruotti, V., Stewart, R.*, et al.* (2007). Induced pluripotent stem cell lines derived
1127 from human somatic cells. Science *318*, 1917-1920. doi: 10.1126/science.1151526.

1128 Zhou, H., Mehta, S., Srivastava, S.P., Grabinska, K., Zhang, X., Wong, C., Hedayat, A., Perrotta,
1129 P., Fernandez-Hernando, C., Sessa, W.C.*, et al.* (2020). Endothelial cell-glucocorticoid receptor
1130 interactions and regulation of Wnt signaling. JCI Insight *5*. doi: 10.1172/jci.insight.131384.
1131

1132